Universidad de Cantabria

Facultad de Ciencias

First-principles study of the phase transitions in perovskites associated with octahedral rotations

(Estudio desde primeros principios de transiciones de fase asociados a rotaciones de los octaedros en perovskitas)

Trabajo de Fin de Grado
para acceder al

GRADO EN FÍSICA

Autor: Mikel Solaguren Anaut

Director: Pablo García Fernández

Julio - 2025

Agradecimientos

Quiero comenzar agradeciendo sinceramente a mi director de TFG, Pablo García. La realización de este trabajo habría sido imposible sin su ayuda. Su infinita paciencia para explicarme los conceptos hasta que los comprendía, así como su profundo conocimiento de la física, no solo me han permitido completar este proyecto, sino que también me han hecho aprender y disfrutar del proceso.

Además, le agradezco especialmente su comprensión en los momentos en que no pude asistir a reuniones debido a otros trabajos o exámenes. Incluso tras semanas sin poder vernos, lo primero que hacía era interesarse por cómo me habían ido los exámenes o los proyectos, algo que valoro mucho.

También quiero dar las gracias a mis amigos, tanto de Santander como de Getxo, por su apoyo y compañía a lo largo de estos años. En especial, a quienes he tenido la suerte de compartir piso durante la carrera: Pablo, Pablin, Pepe y Emilio. Gracias por hacer que mi estancia en Santander haya sido tan buena y llena de buenos momentos. Quiero agradecer por otro lado a mis "compañeros de piso" Paula y Josu por acogerme cada día en su casa, donde he llegado a pasar casi tanto tiempo como en la mía.

Agradezco también de corazón el apoyo de mi familia. Gracias a mis padres, Espe y Txokobo, por creer en mí y acompañarme en cada paso a lo largo de la carrera. Su confianza y ánimo han sido fundamentales. También quiero dar las gracias a mi hermano Asier, que ha tenido que aguantarme durante todos estos años.

Por último, quiero dar las gracias a mi tía Isa y a mi amigo Aitor, quienes, tras leer los agradecimientos de mi TFG de Matemáticas, pidieron ser expresamente mencionados en el siguiente.

Abstract

Perovskites are a class of crystals of chemical formula ABX_3 that can be visualized as a network of BX_6 octahedra connected by the vertices, with the A-cation sitting in the interstices between octahedra. These crystals have an ideal cubic structure that often deforms into lower symmetry structures. The most common deformation, is the one in which the BX_6 octahedra rotate. The main focus of this work is the analysis of these rotations. In order to do this, a model based on Ginzburg-Landau theory is developed to study the highly anharmonic potential energy surface of perovskites undergoing octahedral rotations. The model, rooted in symmetry and group theory, is complemented by first-principles calculations of the potential energy and relaxed atomic structures for three representative compounds: $NaTaO_3$, $LaAlO_3$, and $SrTiO_3$. To characterize the stability of different octahedral rotations, the contributions of individual energy surface coefficients are systematically analyzed. By combining the theoretical model with numerical results, this study provides an explanation for the prevalence of the *Pnma* tilt system in perovskites and offers insight into the critical role played by A-site cation displacements in stabilizing specific structural phases.

Key words: Perovskite, octahedral rotation, first-principles, symmetry

Resumen

Las perovskitas son un tipo de cristal de formula química ABX_3 que se pueden visualizar como una red de octaedros BX_6 conectados por los vértices, con el cation A en el intersticio entre los octaedros. Estos cristales tienen una estructura ideal cúbica que comunmente se deforma en estructuras de menor simetría. La deformación más común son las rotaciones de los octaedros BX_6. El objetivo principal de este trabajo es el análisis de estas rotaciones. Para hacer esto, se ha desarrollado un modelo basado en la teoría de Ginzburg-Landau para estudiar la superficie de energía potencial altamente anarmónica de perovskitas sometidas a rotaciones octaédricas. El modelo, fundamentado en la simetría y la teoría de grupos, se complementa con cálculos de primeros principios de la energía potencial y las estructuras atómicas relajadas para tres compuestos representativos: $NaTaO_3$, $LaAlO_3$ y $SrTiO_3$. Para caracterizar la estabilidad de las diferentes rotaciones de los octaedros, se analizan sistemáticamente las contribuciones de los coeficientes individuales de la superficie de energía. Al combinar el modelo teórico con los resultados numéricos, este estudio proporciona una explicación de la prevalencia del sistema de rotación *Pnma* en perovskitas y ofrece una visión sobre el papel crítico que juegan los desplazamientos del catión A en la estabilización de fases estructurales específicas.

Palabras clave: Perovskita, rotación octaédrica, primeros principios, simetría

Contents

Chapter 1

Introduction

In modern material physics, perovskites are one of the most studied materials due to their wide range of properties and applications [1–5]. Perovskites are a class of materials that have a specific crystal structure and chemical composition. They are characterized by their ABX_3 chemical formula, where A and B are cations and X is an anion. This apparently simple chemical formula hides a rich variety of structures and properties that make perovskites interesting for a wide range of applications.

The main interest and variety of properties of perovskites comes from the fact that their ideal structure is a high-symmetry cubic structure that can easily distort into a wide variety of lower symmetry structures. Depending on the distortion and the initial electronic structure, the deformed perovskites can exhibit many different properties such as ferroelectricity [1], piezoelectricity [2], superconductivity [3],ferro or antiferro magnetism [4] or photocatalytic activity [5]. These properties make perovskites interesting for a wide range of applications such as sensors, actuators, solar cells, batteries or catalysts [6].

It is due to the wide range of properties that technologies using perovskites are constantly being developed. For example, hybrid organic-inorganic perovskites such as $CH_3NH_3PbI_3$ are being studied for their potential use in solar cells [6]. In fact, this hybrid perovskite has shown to have an efficiency of 26.7-34.6% in power conversion [7].

As the macroscopic properties of perovskites change depending on the crystal structure, it is important to understand how the crystal structure of perovskites can change and the way external perturbations influence this structure. The main goal of this work is to develop a symmetry-based model to study the stability of different perovskite structures under a typical distortion usually called octahedral rotation or tilting. Then, *ab initio* or first principle methods are used to obtain reliable numerical data to compare to the model.

1.1 The perovskite structure and practical applications

Perovskite crystals have a ABX_3 chemical formula where A and B are cations and X is an anion which in the case of the three crystals studied in this work, is oxygen.

Perovskites have an ideal cubic structure that belongs to the $Pm\bar{3}m$ space group. In this structure, the B-cations are located at the corners of the cube that forms the unit cell, the A-cations are located at the center of the cube and the X-cation are located in the middle of the edges of the cube. This structure is shown in Fig. 1.1.

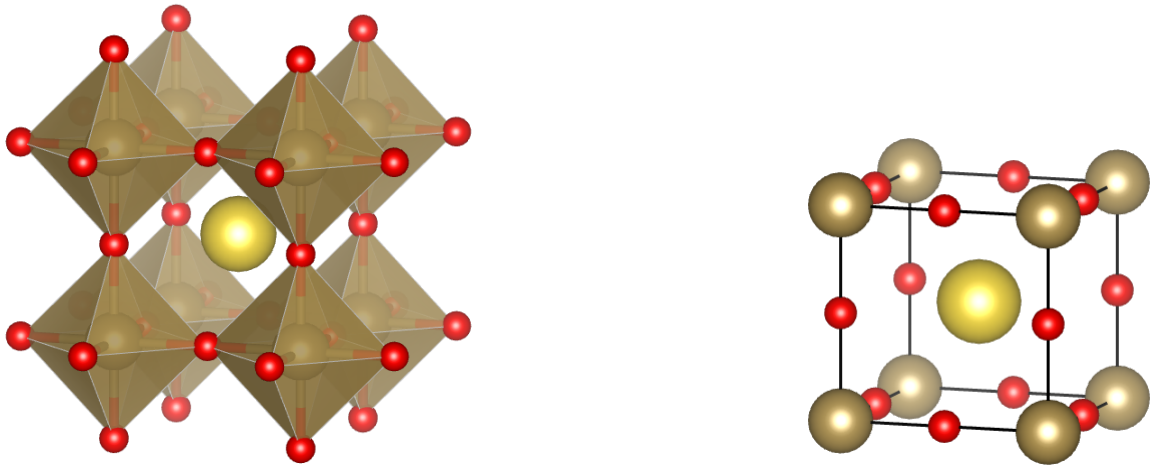

Figure 1.1: This figure shows the cubic $Pm\bar{3}m$ configuration of a typical ABX_3 perovskite. The figure is obtained using the software VESTA [8]. The red spheres represent the X-ions, the brown ones the B-ions and the yellow one the A-ion. The figure in the left is the visualization of the octahedra while the figure on the right is the visualization of the unit cell.

Despite the ideal structure being a high-symmetry cubic structure, perovskites often undergo distortions to lower symmetry structures due to a combination of their chemical compositions [9] and/or physical conditions, such as temperature or pressure [10]. There are three typical ways in which perovskites can distort: A or B ion displacement, octahedral deformation and octahedral tiltings [11]. Despite being three distinct distortions that lower the symmetry, they are not mutually exclusive and can occur simultaneously in the same crystal although this is not overly common.

A or B ion displacement is the phenomena where the A and B cations are displaced off-center from their ideal positions in the crystal structure (i.e. their positions in the high symmetry cubic phase). This displacement can be caused by different factors, such as chemical preference for less, but stronger bonds or physical, like the application of an external electric field. The displacement of the cations can lead to a distortion of the crystal structure and a change in the properties of the perovskite. Most remarkably, the displacement of the cations can lead to the formation of a dipole moment in the crystal and ferroelectricity. Some notable examples of perovskites that exhibit ion displacement and ferroelectricity are $BaTiO_3$ [12], $PbTiO_3$ [1] and $KNbO_3$ [13]. An example of the B-ion displacement is shown in Figure 1.2.

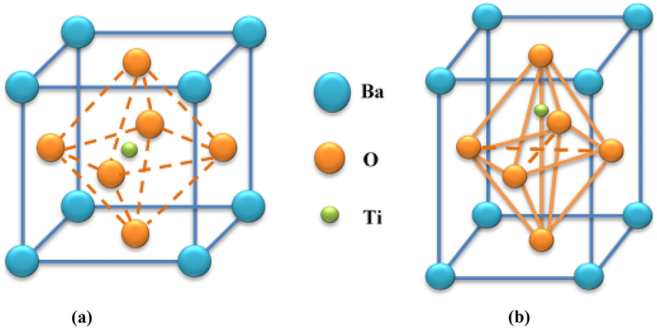

Figure 1.2: This figure shows the B-ion displacement, in green, in $BaTiO_3$ perovskites. The electric dipole would be oriented along the vertical axis of the image. This figure is taken from [14].

Octahedral deformation is the phenomenon where the octahedra are distorted either by changes in the

B-X bond lengths or by variations in the X-B-X bond angles. These distortions can significantly affect the properties of perovskites, such as the band gap or the dielectric constant. In some systems, such deformations arise from the *cooperative Jahn-Teller effect* (cJT), where orbital degeneracy of B-site cations such as Cu^{2+} in $KCuF_3$ leads to collective distortions of adjacent octahedra throughout the lattice [15]. Examples of perovskites that display this kind of deformations are $KCuF_3$ [15] or $La_{1-x}Sr_xMnO_3$ [16]. Although this work does not focus on such mechanisms, they illustrate how structural effects can couple to electronic degrees of freedom in perovskites. An example of the octahedral deformations can be seen in Figure 1.3.

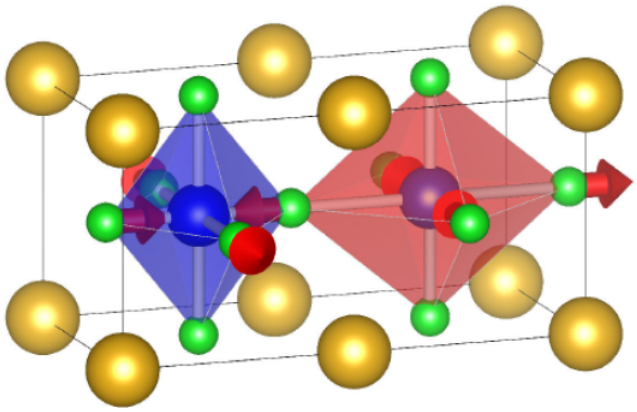

Figure 1.3: This figure shows the octahedral deformation and the cooperative Jahn-Teller effect in perovskites such as $KCuF_3$. This figure is taken from [17].

Octahedral rotations are the phenomena where the BX_6 octahedra tilt around the X, Y and Z axes of the ideal cubic structure. The tilting of the octahedra can lead to a distortion of the crystal structure and a change in the properties of the perovskite such as their magnetic behavior [18]. Some notable examples of perovskites that exhibit octahedral tiltings are $LaAlO_3$ [19] or $CaTiO_3$ [20]. This type of distortions are the main focus of this work and will be further explained in Section 1.2. An example of the octahedral rotations can be seen in Figure 1.4.

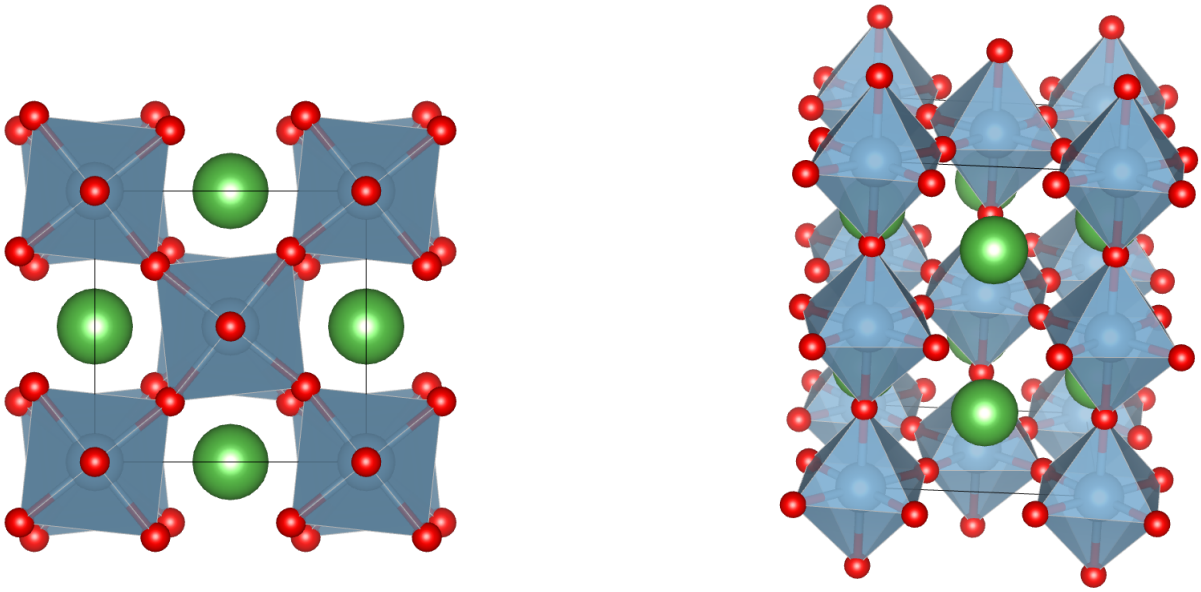

Figure 1.4: Representation of the octahedral tiltings in $LaAlO_3$ using VESTA [8]

1.2 Octahedral tiltings

Among the three kinds of distortions perovskites can have, tiltings are the most common and the richest in terms of properties. The earliest observations of octahedral tiltings go back to H.D.Megaw [21]. However, it was A.M.Glazer [22] who first classified the different types of octahedral tiltings in perovskites. In his work, Glazer classified the octahedral tiltings in perovskites in two different categories depending on the direction of rotation of the next octahedra along the axis of rotation. Glazer proposed that a triplet $a^*b^*c^*$ is enough to describe all the tiltings of perovskites. The letters represent the amount of rotation along the [100], [010] or [001] directions of the $Pm\bar{3}m$ cubic structure and the superscript $*$ indicates whether the rotation of the next octahedra is in the same direction (+), in the opposite direction (-) or if theres no rotation at all in that direction (0) (see Fig. 1.5 for the difference between in-phase (+) and out-of-phase (-) tiltings).

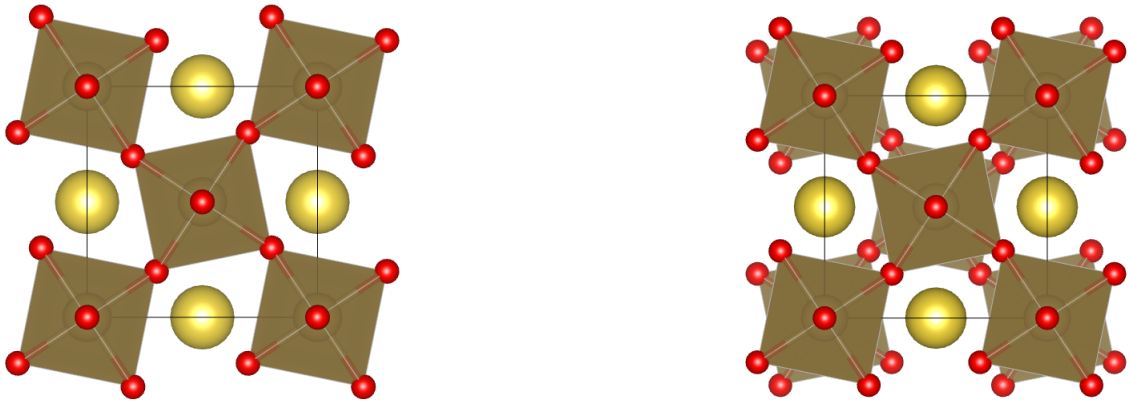

Figure 1.5: Representation of the octahedral tiltings in-phase $c^+a^0a^0$ in the right figure and out-of-phase $c^-a^0a^0$ in the left figure. In this work, in-phase tiltings refer to those tiltings where two octahedron, adjacent along the axis of rotation, rotate in the same direction (both clockwise or both anti clockwise). On the other hand, out-of-phase tiltings refer to those tiltings where to octahedron, adjacent along the axis of rotation, rotate in opposite directions. In both of this cases the rotations are the same in magnitude for all octahedra along the axis of rotation. The in-phase rotations have a symmetry corresponding to the M point in the reciprocal lattice and the out-of-phase rotations to the R point [23, 24].

Glazer's classification of the octahedral tiltings allowed him to obtain a list of 23 tilt systems. Later, P.M. Woodward [23] proved that 6 of those configurations cannot be obtained without octahedral distortions. In that same paper [23], Woodward systematically mapped Glazers tilt systems to specific space groups and studied how these distortions affect the positions of the atoms. His work provided a thorough classification of the different tilt systems, particularly by tabulating the different Wyckoff positions of the atoms in the different tilt systems. This classification is still used today and is the basis for the study of octahedral tiltings in perovskites.

In parallel to Woodward, Howard and Stokes [24] developed a complementary approach using group theoretical arguments to classify the different octahedral tiltings in perovskites further reducing Glazer's 23 tilt system list to 15 (see Fig. 1.6).

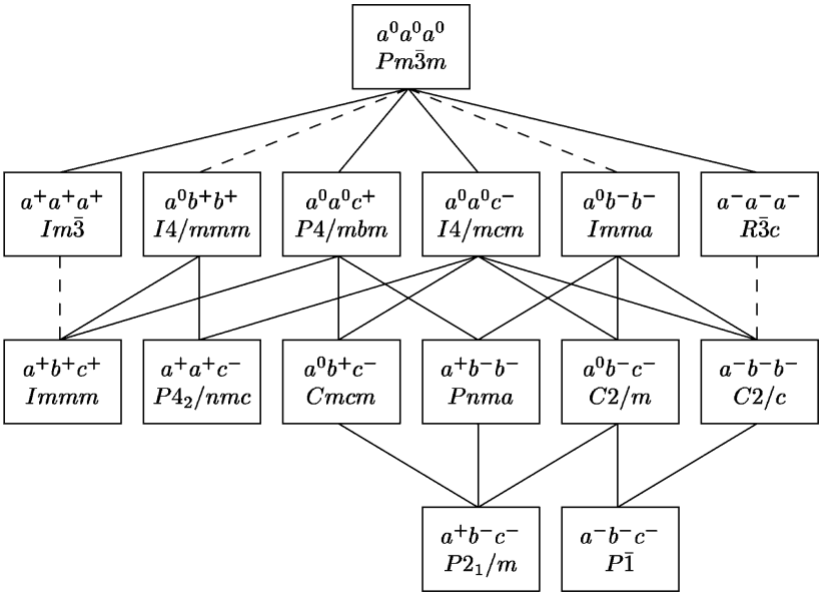

Figure 1.6: This figure shows all 15 tilt systems studied by Howard and Stokes [24]. Each box contains the information about each tilt-system both in Glazers notation and with the respective space-group below. The table is organized in a way where each row adds one more degree of freedom to the tiltings. The lines represent the group-subgroup relation between the tilt-systems and a dashed line represents that the corresponding phase transition is required by Landau theory to be first order [24]

In their work, Howard and Stokes introduce the *order parameter* $\eta = (\eta_1, ..., \eta_6)$ in order to describe Glazer's tilt systems in a more mathematical way. In this work, they consider a basis for a vector space formed by the basic tilt systems

$$\mathcal{B} = \{(c^+a^0a^0), (a^0c^+a^0), (a^0a^0c^+), (c^-a^0a^0), (a^0c^-a^0), (a^0a^0c^-)\} = \{\varphi_1, ..., \varphi_6\} \tag{1.1}$$

Now, the order parameter $\eta = (\eta_1, ..., \eta_6)$ is a 6-tuple where the component η_i is proportional to the angle associated to the basis function φ_i. This way, a tilt system such as $a^+b^-c^-$ can be written as $\eta = (a000bc)$. Despite the change from Gazier's notation to the order parameter notation being subtle, the new way of writing the tilt systems allows for the use of group theory and representation theory to study the different tilt systems. In fact, given a certain symmetry operator $\hat{g}$ with matrix representation $D(g) = \{D(g)_{ij}\}$, the symmetry operation over the tilt system can be written as a simple matrix multiplication:

$$\hat{g}\eta = D(g)\eta = \begin{pmatrix} D(g)_{11} & \cdots & D(g)_{16} \\ \vdots & \ddots & \vdots \\ D(g)_{61} & \cdots & D(g)_{66} \end{pmatrix} \begin{pmatrix} \eta_1 \\ \vdots \\ \eta_6 \end{pmatrix} \tag{1.2}$$

This way, by taking all the symmetry operations of the high symmetry cubic structure, the symmetry operations of a given tilt system η can be obtained by keeping the operations that satisfy the condition $\hat{g}\eta = \eta$. In fact, this approach not only allows to obtain the space group symmetry of a given tilt system, but also allows to obtain the group subgroup relations between the different tilt systems as shown in Fig. 1.6.

Despite this not being the main focus of the work, it is worth mentioning the model proposed by V.M. Goldschmidt [25] in 1926. In his work, Goldschmidt proposes a tolerance factor that depends on the ionic

radii of the A and B cations and the X anion in order to determine whether a given perovskite will have octahedral tiltings or not. This tolerance factor is defined as:

$$t = \frac{r_A + r_X}{\sqrt{2}(r_B + r_X)} \tag{1.3}$$

Where r_A, r_B and r_X are the ionic radii of the A, B and X cations respectively. If Goldschmidt's factor is near in value to one, the perovskite is expected to be stable in the cubic configuration. However, if the tolerance factor is different to one then the perovskite will tend to distort. In particular, if $t < 1$ then octahedral rotations are expected to stabilize the system. Goldschmidt's tolerance factor is usually considered a useful tool to predict whether a given perovskite will have octahedral tiltings or not. However, it is not sustained on rigorous foundations and it produces many erroneous predictions.

Despite many phases being posible (see Fig. 1.6), $Pnma$ is by far the most common tilt system [26] and is known as the structure ReO_3.

1.3 Chosen perovskites

In order to study real systems, three distinct perovskite systems have been chosen for this work. The choice of the systems is based on the fact that all three systems have different stable tilt systems. These compounds are $NaTaO_3$, $LaAlO_3$ and $SrTiO_3$. A brief description of each of the chosen perovskites is given below.

$NaTaO_3$ adopts an orthorhombic structure with space group $Pnma$ and a tilt system $a^+b^-b^-$ at low temperatures [27]. This configuration persists up to above 803K where it undergoes a change in the tilt system and takes the phase $Cmcm$ with a tilt system $a^0b^+c^-$. This phase persists up to 897K where it undergoes a transition to the phase $P4/mbm$ with tilt system $a^0a^0c^+$ [27]. NaTaO3 shows a promising photocatalytic activity for water splitting [28]. It has been chosen for this work because it is represents the most frequent rotation pattern displaying $Pnma$ symmetry. It also displays large octahedral tiltings what makes it easier to study.

$LaAlO_3$ adopts a rhombohedral structure with space group $R\bar{3}c$ and a tilt system $a^-a^-a^-$ at room temperature. This configuration persists up to 798K where the phase becomes cubic with space group $Pm\bar{3}m$ and a tilt system $a^0a^0a^0$ [29]. $LaAlO_3$ is dielectric and has applications as a thermoluminescent or photoluminescent material [30]. One of the reasons why this compound has been chosen is because it has a negative frequency in the phonon dispersion diagram for the point R of the reciprocal lattice [31]. This means that only the in-phase tiltings are unstable at low temperatures (see Fig. 1.5).

$SrTiO_3$ adopts a tetragonal structure with space group $I4/mcm$ and a tilt system $a^0a^0c^-$ at low temperatures. This configuration persists up to 105K where it undergoes a structural phase transition to the cubic phase with space group $Pm\bar{3}m$ and a tilt system $a^0a^0a^0$ [32]. Some relevant properties of $SrTiO_3$ are its usefulness as a semiconductor, its thermoelectric properties [33] and its incipient ferroelectricity [34].

These properties not only make the three chosen perovskites interesting due to their variety in tilt systems, but also due to their different applications in the field of materials science.

1.4 Objectives

The main objective of this work is to model the minimum energy surface of a perovskite involving octahedral tiltings with the help of symmetry and group theory. This approach has been used in the past to classify the different tilt systems in perovskites [23, 24]. However, there exist no systematic studies where these kind of arguments have been used to study the stability of the different phases.

If we assumed the possibility of finding a tilt system to be just dependent on the number of configurations, all tilt systems should be equally probable or at least they should follow some kind of distribution based on the group-subgroup relations. However, this is not the case in real systems. In fact, there is one tilt system that is the most stable for the majority of perovskites, the $Pnma$ or $a^+b^-b^-$ [26]. The main goal of this work is to lay the foundations of a model that explains why some tilt systems are more stable than others. This model will be based on the symmetry of the different tilt systems and the group-subgroup relations between them.

To address this problem, from a quantitative perspective, we base our approach on Ginzburg-Landau theory [35]. This theory is a phenomenological theory that describes the behavior of systems near a phase transition. The Ginzburg-Landau theory is used to study the stability of the different tilt systems and to obtain a quantitative measure of their stability.

In this case, the system's electronic energy is expanded in terms of the different rotations and distortions. This expansion allows to obtain an approximate expression for the energy as a multivariate polynomial. The coefficients of this polynomial are obtained using first principle methods. The stability of the different tilt systems is then studied by analyzing the minimum energy for each phase and comparing it to the others. This shows some relations between the polynomial coefficients that show the importance of the different coefficients in the stability of the different tilt systems.

In order to determine the exact values of the coefficients of the polynomial, first principle methods are used. These methods are based only on the solution of the Schrödinger equation and they do not use any experimental data. This allows to study systems that cannot be studied experimentally. In fact, first principle methods make it posible to study systems that are not stable in the laboratory or that are not easy to synthesize.

Based on this, the objectives of this work can be summarized as follows:

- Develop a Ginzburg-Landau type model to **study the general electronic energy surface** of perovskites.
- Using the model, **determine the relative stability of the different tilt systems** in perovskites and **find a general origin** for said stabilities.
- Gain a further understanding of the model using real perovskites by **first principle methods**.

Achieving these objectives will not only provide a better understanding of the stability of the different tilt systems in perovskites, but also lay the foundations for a theory that can be used to study other materials with similar properties.

1.5 Structure of the work

This work is divided into four distinct chapters. In the first chapter, the introduction, we have provided a brief overview of the perovskite structure and the different types of distortions that can occur in perovskites. It also introduces the three chosen perovskites and the objectives of the work.

The second chapter of the work is the explanation of the computational methods used (see Chapter 2). Here, the theoretical background and approximations needed to understand the computational methods used in this work are explained. The section is divided into two parts; the first one explains the first principle methods used and the second part explains the specific tools and programs used in this work.

The third chapter is the main part of the work (see Chapter 3). In this section, the results are shown and discussed. The section is divided into two parts. First, the theoretical energy model for the perovskites is introduced and derived. The second part of the section is dedicated to further understanding the model using data from first principle simulations.

Finally (see Chapter 4), to conclude the work, a summary of the results is given and the conclusions are presented. In this section, future work is also proposed in order to further understand the stability of the different tilt systems in perovskites.

Chapter 2

Computational methods

This chapter gives a detailed explanation of the theoretical background needed to understand the computational methods used in this work, as well as a description of the specific tools and programs used.

2.1 First principle methods

The goal of this work is to study the molecular structure and properties of perovskites. To do this, one must solve the Schrödinger equation for the system given by:

$$\hat{H}\Psi(\{\vec{r}\},\{\vec{R}\},t) = E\Psi(\{\vec{r}\},\{\vec{R}\},t) \tag{2.1}$$

This equation is, in general, unsolvable analytically and thus numerical methods are required. This section introduces the concepts and approximations needed to solve the Schrödinger equation numerically. The methods used in this work are called first principle methods (or ab initio methods) which are methods independent from any experimental data other than fundamental physical constants and, can be used to study systems in conditions that cannot otherwise be studied experimentally.

This is a heavily theoretical section and, for most of the methods introduced here, some of the details on the proofs are omitted as they are not the main focus of the work. The more detailed explanations can be found in the books [36] and [37] which are the main bibliography for the section.

2.1.1 Hamiltonian

The Hamiltonian operator is the operator that describes the total energy of a system and it is defined in its most general form as the sum of the kinetic and potential energy operators. This operators differ depending on the studied system and the approximations made. The objective of this work is to study the molecular structure of perovskites and thus two initial approximations can be made to simplify the terms of the Hamiltonian. The first initial approximation is neglecting the relativistic effects as the relativistic corrections only account for a small fraction of the total energy, especially in the case of light elements. The second initial approximation is considering that the electrons and nuclei only interact through the electrostatic potential, as the strong, weak and gravitational forces are negligible in the molecular scale.

With these initial approximations, the total Hamiltonian operator is a sum of different contributions corresponding to both electrons and nuclei. Supposing that the system consists of n electrons and N nuclei, the position of all the electrons is written as $\{\vec{r}\} = \{\vec{r}_1, \vec{r}_2, ..., \vec{r}_n\}$ and the position of all the nuclei is written as $\{\vec{R}\} = \{\vec{R}_1, \vec{R}_2, ..., \vec{R}_N\}$. The total Hamiltonian operator is thus written as:

$$\hat{H}(\{\vec{r}\},\{\vec{R}\}) = \hat{T}_n + \hat{T}_e + \hat{V}_{ee} + \hat{V}_{nn} + \hat{V}_{en} \tag{2.2}$$

Where $\hat{T}_n$ and $\hat{T}_e$ represent the kinetic energy of nuclei and electrons respectively and can be written in terms of the atomic masses M_α and the mass of the electron m as:

$$\hat{T}_n = -\sum_{\alpha=1}^{N} \frac{\hbar^2}{2M_\alpha} \nabla^2_{\vec{R}_\alpha} \tag{2.3}$$

$$\hat{T}_e = -\sum_{i=1}^{n} \frac{\hbar^2}{2m} \nabla^2_{\vec{r}_i} \tag{2.4}$$

The terms $\hat{V}_{ee}$, $\hat{V}_{nn}$ and $\hat{V}_{en}$ represent the electron-electron repulsion, nuclei-nuclei repulsion and electron-nuclei attraction respectively. These can be written in terms of the electron charge e, the atomic numbers Z_α and the vacuum permittivity ε_0 as[1]:

$$\hat{V}_{ee} = \frac{1}{2}\frac{1}{4\pi\epsilon_0} \sum_{i\neq j} \frac{e^2}{|\vec{r}_i - \vec{r}_j|} \tag{2.5}$$

$$\hat{V}_{nn} = \frac{1}{2}\frac{1}{4\pi\epsilon_0} \sum_{\alpha\neq\beta} \frac{Z_\alpha Z_\beta e^2}{\left|\vec{R}_\alpha - \vec{R}_\beta\right|} \tag{2.6}$$

$$\hat{V}_{en} = -\frac{1}{2}\frac{1}{4\pi\epsilon_0} \sum_{i,\alpha} \frac{Z_\alpha e^2}{\left|\vec{r}_i - \vec{R}_\alpha\right|} \tag{2.7}$$

It is interesting to note that since the Hamiltonian is time independent the wave functions that describes the system can be written as:

$$\Psi(\{\vec{r}\},\{\vec{R}\},t) = \Psi(\{\vec{r}\},\{\vec{R}\})e^{-i\frac{E}{\hbar}t} \tag{2.8}$$

Where $\Psi(\{\vec{r}\},\{\vec{R}\})$ is an eigenfunction of the Hamiltonian and can be determined as a solution to the time independent Schrödinger equation:

$$\hat{H}\Psi(\{\vec{r}\},\{\vec{R}\}) = E\Psi(\{\vec{r}\},\{\vec{R}\}) \tag{2.9}$$

The system described by this last equation is a many-body system and thus an analytical solution can only be obtained for the two body system (i.e. the hydrogen atom). Considering even the simplest molecules makes the analytical solution impossible and thus numerical methods are needed to solve the time independent Schrödinger equation. These methods are explained in the following sections.

[1]The factor of $\frac{1}{2}$ is included to avoid double counting

2.1.2 Born-Oppenheimer approximation

The Born-Oppenheimer approximation is one of the most basic approximations used in quantum chemistry in order to obtain numerical solutions to the time independent Schrödinger equation (2.9). This approach approximates the problem in a way where the nuclear and electronic motions are solved separately[2]. Moreover, this method solves the problem by solving a smaller electronic problem for each nuclear configuration vastly reducing the computational cost required to solve the Schrödinger equation.

Before making any approximations, the time independent Schrödinger equation has to be rewritten in a way that the electronic and nuclear contributions are separated. This separated expression takes the form:

$$\hat{H}(\{\vec{r}\},\{\vec{R}\}) = \hat{T}_n + \hat{H}_e \tag{2.10}$$

Where $\hat{H}_e(\{\vec{r}\},\{\vec{R}\}) = \hat{T}_e + \hat{V}_{ee} + \hat{V}_{nn} + \hat{V}_{en}$ is the electronic Hamiltonian that only depends on the electronic and nuclear positions and not the nuclear momentum. With this in mind, the electronic wave functions are defined as the eigenstates of the electronic Hamiltonian for each fixed nuclear configuration:

$$\hat{H}_e(\{\vec{r}\},\{\vec{R}\})\Psi_e^{(i)}(\{\vec{r}\};\{\vec{R}\}) = E_e^{(i)}(\{\vec{R}\})\Psi_e^{(i)}(\{\vec{r}\};\{\vec{R}\}) \tag{2.11}$$

Where $\Psi_e^{(i)}(\{\vec{r}\};\{\vec{R}\})$ denotes that the eigenfunction depends explicitly on electronic positions and parametrically in nuclear positions [37]. The electronic energy of the state i is defined as the following integral over all electronic positions and for a given nuclear configuration:

$$E_e^{(i)}(\{\vec{R}\}) = \left\langle \Psi_e^{(i)} \middle| \hat{H}_e \middle| \Psi_e^{(i)} \right\rangle \tag{2.12}$$

As the electronic wave functions form a base over the electronic coordinates, the total wave function can be written as an expansion over the electronic states where the coefficients are functions of the nuclear positions [36]. These coefficients are called nuclear wave functions. The total wave function can thus be written in terms of the nuclear and electronic wave functions as:

$$\Psi(\{\vec{r}\},\{\vec{R}\}) = \sum_i \chi_n^{(i)}(\{\vec{R}\})\Psi_e^{(i)}(\{\vec{r}\};\{\vec{R}\}) \tag{2.13}$$

Substituting the expressions (2.10) and (2.13) in the equation (2.9), operating taking into account the definitions of the terms of the Hamiltonian and multiplying the equation by the complex conjugate of the wave function in the state j, $(\Psi_e^{(j)})^*$, the following equation is obtained:

$$\hat{T}_n\chi_n^{(j)} + E_e^{(j)}\chi_n^{(j)} + \sum_i \left\langle \Psi_e^{(j)} \middle| \hat{T}_n \middle| \Psi_e^{(i)} \right\rangle \chi_n^{(i)} = E\chi_n^{(j)} \tag{2.14}$$

Until this point, no approximations have been made and everything is exact. The Born-Oppenheimer approximation states that as the velocity of the nuclei is much smaller than the velocity of the electrons, the electronic wave function instantly adjusts to the nuclear motion. This condition can be expressed in therms of the nuclear momentum operator as:

$$\hat{P}_n \left| \Psi_e^{(i)} \right\rangle = 0 \Rightarrow \hat{T}_n \left| \Psi_e^{(i)} \right\rangle = 0 \tag{2.15}$$

[2]The fact that the motions are solved separately does not mean they are decoupled. The electronic motion is still affected by the nuclear motion and vice versa.

Applying the Born-Oppenheimer approximation to the equation (2.14) the following equation is obtained:

$$(\hat{T}_n + E_e^{(j)}(\{\vec{R}\}))\chi_n^{(j)}(\{\vec{R}\}) = E\chi_n^{(j)}(\{\vec{R}\}) \tag{2.16}$$

Where the term $E_e^{(j)}(\{\vec{R}\})$ acts as a potential energy for the nuclear motion. This term is called the adiabatic potential energy surface (APES).

As a direct consequence of the approximation, the nuclear wave functions depend only on a single electronic state[3]. This is the reason why this approximation is only valid when the electronic states are well separated in energy. If the electronic states are close in energy the real system might be inclined to mix the electronic states and thus the Born-Oppenheimer approximation is not valid.

2.1.3 Hartree-Fock method

The Hartree-Fock or self consistent field method is a variational method used to solve the electronic Schrödinger equation. This method is based on the assumption that the electronic wave function can be written in terms of the individual one electron wave functions. These one electron wave functions take the form:

$$|\varphi_i(\vec{r})\rangle = |\phi_i(\vec{r})\rangle \otimes |\chi_i\rangle \tag{2.17}$$

Where $|\phi_i(\vec{r})\rangle$ is the spatial part of the wave function and $|\chi_i\rangle$ is the spin part of the wave function. The wave functions that take the form of the equation (2.17) are called molecular orbitals.

In order to explain Pauli's exclusion principle, a suitable expression for the wave function in terms of the one electron wave functions must be antisymmetric with respect to the permutation of two electrons. This antisymmetry is achieved by writing the wave function as a Slater determinant of the one electron wave functions:

$$\Psi(\vec{r}_1, \vec{r}_2, ..., \vec{r}_n) = \frac{1}{\sqrt{n!}} \begin{vmatrix} \varphi_1(\vec{r}_1) & \varphi_2(\vec{r}_1) & \cdots & \varphi_n(\vec{r}_1) \\ \varphi_1(\vec{r}_2) & \varphi_2(\vec{r}_2) & \cdots & \varphi_n(\vec{r}_2) \\ \vdots & \vdots & \ddots & \vdots \\ \varphi_1(\vec{r}_n) & \varphi_2(\vec{r}_n) & \cdots & \varphi_n(\vec{r}_n) \end{vmatrix} \tag{2.18}$$

With the introduction of the Slater determinant it is easy to see how if two identical wave functions are introduced ($\varphi_i = \varphi_j$), then the total wave function is zero, verifying Pauli's exclusion principle.

For the obtention of the Hartree-Fock equations, it is useful to rearrange the electronic Hamiltonian in a way where different terms have different electron indices. The electronic Hamiltonian can thus be written as:

$$\hat{H}_e = V_{nn} + \sum_{i=1}^{n} \hat{h}_i + \frac{1}{2}\sum_{i=1}^{n}\sum_{j=1}^{n} \hat{g}_{ij} \tag{2.19}$$

Where the operators $\hat{h}_i$ and $\hat{g}_{ij}$ are defined as:

$$\hat{h}_i = -\frac{1}{2}\nabla_i^2 - \sum_{\alpha} \frac{Z_\alpha}{|\vec{r}_i - \vec{R}_\alpha|} \tag{2.20}$$

[3]This is because the mixed term in the equation (2.14) is neglected.

$$\hat{g}_{ij} = \frac{1}{|\vec{r_i} - \vec{r_j}|} \tag{2.21}$$

With some straightforward but lengthy calculations [36], the expected value of the electronic Hamiltonian in the state described by the Slater determinant can be written as:

$$E = \hat{V}_{nn} + \sum_{i=1}^{n} \hat{h}_i + \frac{1}{2} \sum_{i=1}^{n} \sum_{j=1}^{n} (J_{ij} - K_{ij}) \tag{2.22}$$

Where the terms J_{ij} and K_{ij} are called the Coulomb and Exchange elements and can be written in terms of the Coulomb and Exchange operators as the integrals $\langle \phi_j | \hat{J}_i | \phi_j \rangle$ and $\langle \phi_j | \hat{K}_i | \phi_j \rangle$. These operators are defined by:

$$\hat{J}_i \left| \varphi_j(\vec{r_t}) \right\rangle = \left\langle \varphi_j(\vec{r_k}) | \hat{g}_{kt} | \varphi_j(\vec{r_k}) \right\rangle \left| \varphi_j(\vec{r_t}) \right\rangle \tag{2.23}$$

$$\hat{K}_i \left| \varphi_j(\vec{r_t}) \right\rangle = \left\langle \varphi_i(\vec{r_k}) | \hat{g}_{kt} | \phi_j(\vec{r_k}) \right\rangle \left| \varphi_i(\vec{r_t}) \right\rangle \tag{2.24}$$

The next step is to determine the configuration of molecular orbitals that makes the energy of the system stationary. This problem has the added constraint that the molecular orbitals must remain orthonormal and normalized. The solution to this constrained optimization problem can be found by means of Lagrange Multipliers [36]. This type of process yields a set of n one body equations out of the initial n body single equation. These equations are the Hartree-Fock equations and are written in terms of the Fock operator $\hat{F}_i$ as:

$$\hat{F}_i \varphi_i(\vec{r}) = \epsilon_i \varphi_i(\vec{r}) \tag{2.25}$$

Where the Fock operator is defined as:

$$\hat{F}_i = \hat{h}_i + \sum_{j=1}^{n} \left(\hat{J}_j - \hat{K}_j \right) = -\frac{1}{2} \nabla_i^2 - \sum_{\alpha} \frac{Z_\alpha}{|\vec{r_i} - \vec{R}_\alpha|} + \sum_{j=1}^{n} \left(\hat{J}_j - \hat{K}_j \right) \tag{2.26}$$

This operator acts as a one electron Hamiltonian where the potential energy is given as an average of all the individual Coulomb potentials generated by all electrons. This is why a specific one electron wave function can only be obtained if all the other one electron wave functions are known and thus the Hartree-Fock equations are solved self-consistently, hence the name self-consistent field (SCF) method.

2.1.4 Density Functional Theory

The Density Functional Theory (DFT) is a method used to solve the electronic Schrödinger equation by means of the electron density instead of the wave function. This method is based on the Hohenberg-Kohn theorems [38] and the Kohn-Sham equations [39]. The first Hohenberg-Kohn theorem states that "the electron density in fact uniquely determines the Hamilton operator and thus all properties of the system" [40] and the second Hohenberg-Kohn theorem states that "the functional that delivers the ground state energy of the system, delivers the lowest energy if and only if the input density is the true ground state density" [40]. In other words, the ground state energy of a system can be determined by minimizing the energy functional with respect to the electron density. This approach allows the ground state energy to be determined without the need of the wave function and needing only the electron density which depends

on three spacial coordinates regardless of the number of electrons. The main obstacle this method faces is the determination of the energy functional which is unknown and must be approximated.

Within the framework of the Born-Oppenheimer approximation, the energy functional in terms of the electronic density can be written as:

$$E[\rho] = T[\rho] + E_{ee}[\rho] + E_{ne}[\rho] \tag{2.27}$$

Where $T[\rho]$ is the kinetic energy of the electrons, $E_{ee}[\rho]$ is the electron-electron repulsion energy and $E_{ne}[\rho]$ is the electron-nuclei attraction energy. Furthermore, using the Hartree-Fock approximation, the electron-electron repulsion energy can be separated in a Coulomb and an Exchange term as:

$$E[\rho] = T[\rho] + J[\rho] + K[\rho] + E_{ne}[\rho] \tag{2.28}$$

The electron-nuclei attraction term and the Coulomb term can be written in terms of the electron density using classical electrostatics as:

$$E_{ne}[\rho] = -\sum_{\alpha} \int \frac{Z_\alpha \rho(\vec{r})}{|\vec{r} - \vec{R}_\alpha|} d\vec{r} \tag{2.29}$$

$$J[\rho] = \frac{1}{2} \int \int \frac{\rho(\vec{r})\rho(\vec{r'})}{|\vec{r} - \vec{r'}|} d\vec{r} d\vec{r'} \tag{2.30}$$

Thus, the problem of DFT is reduced to finding the right Exchange and kinetic energy functionals. The first approach to this problem was made by Thomas [41] and Fermi [42] who proposed a functional for the kinetic energy of the electrons. This functional is called the Thomas-Fermi functional. This functional neglected the Exchange term and proposed a non-interacting uniform electron gas model in order to obtain the kinetic energy of the electrons. Later, Bloch [43] and Dirac [44] proposed a functional for the Exchange term. The results calculated from those functionals however had errors of $15 - 50\%$ and failed to predict bonding at all [36].

The modern DFT was developed by Kohn and Sham [39] who proposed a new method to compute the kinetic energy functional, which is the term that affects the results the most. The Kohn-Sham method consists on computing the kinetic energy as a term from a non interacting electron gas plus a correlation term that accounts for the difference between the non interacting electron gas and the real system as well as all the non classical effects.

Since the exact wave functions of a non interacting electron gas are Slater determinants [40], a non interacting reference system can be set up where a local potential $V_S(\vec{r})$ is introduced:

$$\hat{H}_S = -\frac{1}{2} \sum_i \nabla_i^2 + \sum_i V_S(\vec{r_i}) \tag{2.31}$$

Since the Hamiltonian does not have electron-electron interaction terms, the wave functions of this system are Slater determinants and following a similar process as in the previous section a set of one electron equations can be obtained. These equations are called the Kohn-Sham equations and are written as:

$$\hat{h}_{KS}\varphi_i(\vec{r}) = \epsilon_i \varphi_i(\vec{r}) \tag{2.32}$$

Where the functions $\{\varphi_i\}$ are called the Khon-Sham orbitals and $\hat{h}_{KS}$ is the Khon-Sham operator defined as:

$$\hat{h}_{KS} = -\frac{1}{2}\nabla_i^2 + V_S(\vec{r_i}) \tag{2.33}$$

The connection from this system to the real system is made by setting the electron density of the real system equal to the electron density of the non interacting reference system. This is shown in the following equation (where the spin states are also taken into account):

$$\rho_S(\vec{r}) = \sum_i^n \sum_s |\varphi_i(\vec{r}, s)|^2 = \rho_0(\vec{r}) \tag{2.34}$$

Considering this reference change, the energy functional can be written as:

$$E[\rho] = T_S[\rho] + E_{ee}[\rho] + E_{ne}[\rho] + E_{xc}[\rho] \tag{2.35}$$

Where $T_S[\rho]$ is the kinetic energy of the non interacting reference system, and $E_{xc}[\rho]$ is term that accounts for the difference between the ideal and real kinetic energies as well as for the non classical effects. This last term is defined as:

$$E_{xc}[\rho] = (T[\rho] - T_S[\rho]) + (E_{ee}[\rho] - J[\rho]) \tag{2.36}$$

Where the first parenthesis can be considered as the kinetic correlation energy while the second contains both exchange and potential correlation energy. If the exact form of the functional $E_{xc}[\rho]$ was known, DFT would be an exact method. Since the term E_{xc} and thus the potential V_S are unknown, solving the constrained optimization problem it can be obtained that the potential V_S has the form:

$$V_S(\vec{r}) = \int \frac{\rho(\vec{r}_2)}{r_{12}} d\vec{r}_2 + \frac{\delta E_{xc}}{\delta \rho} - \sum_\alpha^M \frac{Z_\alpha}{r_{1\alpha}} \tag{2.37}$$

Which is written in terms of the functional derivative of the unknown E_{xc}. The only unknown term is this last derivative but the exchange coefficient has a small effect over the ground energy making this method effective despite not being exact. In practice, a certain effective potential has to be given of the form (2.37). From this point, the Kohn-Sham orbitals can be calculated through the equation (2.32). Lastly, the electronic density can be calculated using the Kohn-Sham orbitals using the relation (2.34) and this density can be used to calculate the ground energy thanks to the equation (2.35).

2.2 Simulation programs: CRYSTAL & VESTA

For the numerical simulations and the interpretation of the geometries two programs have been used: CRYSTAL [45] and VESTA [8].

CRYSTAL is a program that implements all the approximations considered in Section 2.1 and allows to calculate the minimum energy configuration of a system as well as the atomic positions (amongst other things that are not used in this work).

The program uses localized Gaussian basis to describe the electronic wave functions. For this work, the program has been used to calculate the minimum energy configuration of the perovskites from a particular

space group. To do this, the program uses an iterative process, based on DFT, to find the minimum energy configuration of a given system. The iterative process stops when the steps in electronic density, force and atomic displacement are below a certain threshold. Then, the program outputs the minimum energy per unit cell, the atomic positions of the optimal configuration and more information about the system and the process that is not used in this work.

For the particular case of this work, the B1WC density functional has been used as it is the most suitable functional for the study of octahedral rotations in perovskites [46]. The numerical calculations performed by the program need to discretize the reciprocal space. In this work, an 8-8-8 sampling has been used. This means that the each axis of the reciprocal space has been discretized in 8 points.

In order to use the program, the user must input a file where the initial atomic positions, the initial lattice constant and the Gaussian basis are defined. The user also has to specify which functional to use and the sampling of the reciprocal space.

On the other hand, VESTA is a program used to visualize the atomic structures and positions of the systems. In this work, once the optimal configurations for the perovskites are obtained, the geometries are visualized using VESTA. This program allows to determine inter atomic distances, angles and other geometric properties of the system. It also allows to visualize the crystal structure in a 3D environment and to export the structure in different formats.

In order to use VESTA, the user must input the atomic positions, the lattice constants and the space group of the system. The program then visualizes the structure in a 3D environment and allows to manipulate the structure to visualize it from different angles.

Chapter 3

Results and Discussion

In this chapter the theoretical and computational results of the work are explained. First, a theoretical model is proposed as a way to understand the complex energy landscape in perovskite crystals. The parameters in this model are rigorously calculated using first-principle methods. The second part of this chapter is dedicated to the obtention and interpretation of the parameters from the numerical simulations. Finally, using the results from the numerical simulations, the model is used to stablish relations between the values of the parameters and the stable phases of the crystal.

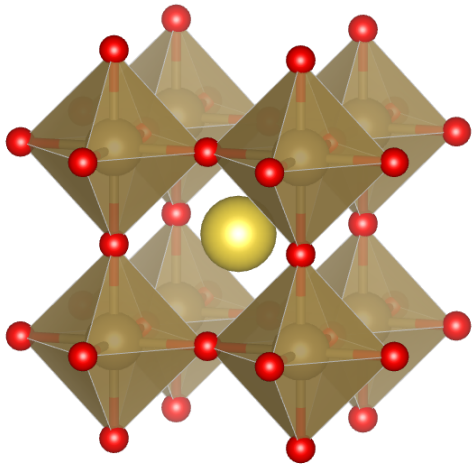

Figure 3.1: This figure shows the cubic $Pm\bar{3}m$ configuration of the perovskite. The figure is obtained using the software VESTA [8]. The red spheres represent the X-ions, the brown ones the B-ions and the yellow one the A-ion. A set of coordinates can be defined in this configuration where the X, Y and Z axises go along the lines formed by the B-ions.

The structure of this chapter and the logic behind the procedure followed here is given next:

- Following typical schemes in-phase transitions in molecular and condensed matter physics [35, 47] our starting point will be a high-symmetry phase. Perovskites of formula ABX_3 have an undistorted, cubic high-symmetry phase that belongs to the $Pm\bar{3}m$ space group (see Fig. 3.1). This is at the top of the octahedral rotation table provided by Howard and Stokes [24] and represented in Fig.3.2. This diagram is the base for the whole analysis carried in this work.

- We will consider the Pm-3m cubic phase with lowest energy. Studying the vibrations associated to this

structure one can find that some normal modes, that usually would be connected with the phonons of the crystal, display a negative force constant, i.e. the cubic phase represents an unstable equilibrium. Thus, these modes correspond with distortions that, if followed, would reduce the energy below the Pm-3m structure. The most important of these distortions are the octahedral rotations of BX_6 complexes and Fig. 3.2 offers a map of the different phases that are produced by these instabilities.

- With the help of symmetry (group theory) we will produce a model energy surface with the goal of determining which combination of modes more strongly stabilize the system. A strong emphasis will be placed on the anharmonic coupling that exists between the modes and we will find that in most cases the phases predicted by Howard and Stokes (Fig. 3.2) involve distortion modes that are not necessarily the octahedral rotations. These modes that deform the octahedra or that involve displacements of the A-ions in a perovskite. We will assess, in Subsection 3.3.2 and Section 3.4, the importance of the different distortions and find the important role that some of them (A-ions motion) have in stabilizing the system.

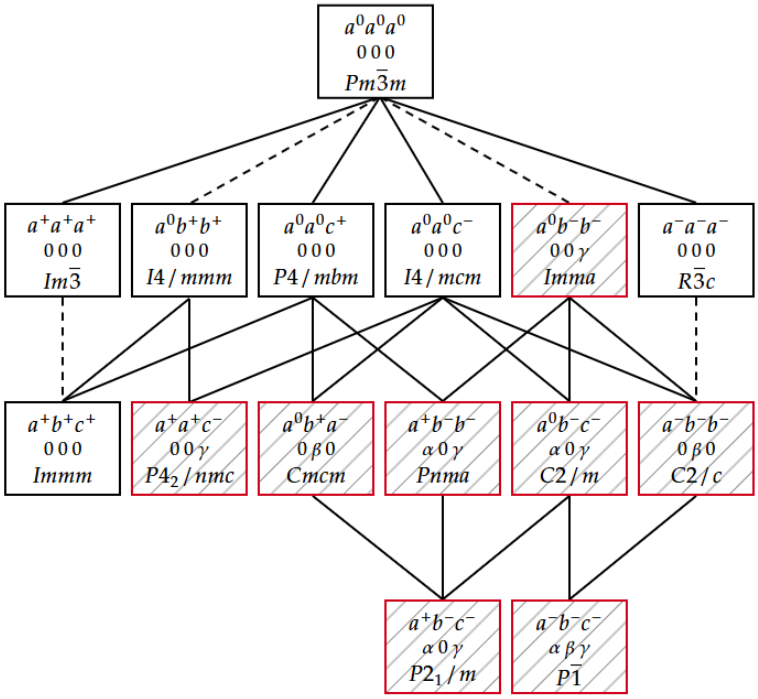

Figure 3.2: This table completes Howard's table (Ref. [24], Fig. 1.6) by adding the movement of the A-ion. The phases in red represent those phases where A is able to move. The indices below Gazier's numbers represent the possible movements of the ion in different directions. This table has been made by using the information about the A-ion in Woodward's paper [23].

3.1 Modeling of energy surface using the symmetry of the system

This section explains the process followed to **obtain the model that describes the energy surfaces of perovskites**. The electronic energy of a certain molecule or solid can be expressed as a function of the nuclear positions. This function is called the potential energy surface and it is the main object of study in this work. Knowing the form of the potential energy surface allows to compute the minimum energy configuration of the system and thus the equilibrium geometry of the system (i.e. knowing the potential energy surface allows to know all the stable configurations of the system). However, in general, the potential energy surface is unknown and must be approximated. The energy surface of a system depends on $3N$ coordinates where N is the number of atoms in the system. However, as mentioned in the introduction of the chapter, when the cubic $Pm\bar{3}m$ phase is taken as a reference, we have found that the tilting modes are

usually unstable and thus we need to follow them to stabilize the system. We have also found (see Subsection 3.2.2 and Section 3.4) that the A-ion displacements are also important. Thus we have 9 coordinates, 6 for the octahedral rotations and 3 for the A-ion displacements. The main problem to solve now is to study the general form of the energy surface.

By means of the Born-Oppenheimer approximation (see Subsection 2.1.2), the energy surface can be written as:

$$E(\{\vec{R}\}) = \langle\Psi|\hat{H}_e|\Psi\rangle \tag{3.1}$$

However, in order to characterize the system by the octahedral tiltings and the A-ion movement, the energy surface must be rewritten as a function of these new distortion coordinates $\{Q_i\}$. This can be done taking advantage of the fact that the energy surface can be expanded as a Taylor series around the unstable cubic configuration where all of the coordinates are zero.

$$E(\{Q_i\}) = E_0 + \sum_i \langle\Psi|\frac{\partial H}{\partial Q_i}|\Psi\rangle\, Q_i + \frac{1}{2}\sum_{i,j} \langle\Psi|\frac{\partial^2 H}{\partial Q_i \partial Q_j}|\Psi\rangle\, Q_i Q_j + ... \tag{3.2}$$

The integrals in this expression cannot be calculated analytically and thus must be approximated numerically. This is why an approximation has to be made not only in order to compute the integrals but also to stop the Taylor expansion at a certain order. Since the reference structure $Pm\bar{3}m$ is a critical point, all forces are zero and therefore the linear terms in equation 3.2 must be zero. On top of that, by a symmetry argument (see Subsection 3.1.1), it can be shown that all odd order terms in the Taylor expansion must also be zero. Therefore, as the quadratic term is negative because the cubic phase is unstable, in order to study the stabilization of the different phases at least the quartic term must be considered.

This Section is separated in two distinct parts:

1. **Vanishing integrals using symmetry arguments:** In this part the justification is given for the different methods used to prove that certain terms in Equation (3.2) vanish. This methods are explained without specifying the system.

2. **Obtaining the reduced energy surface:** In this part the different methods explained in Subsection 3.1.1 are used to obtain the reduced energy surface of the system for the specific case of the perovskites.

3.1.1 Vanishing integrals using symmetry arguments

The problem now is to reduce the unknown integrals to a point where they can be calculated by means of first principle simulations. To do this, the symmetry of the system must be taken into account. Three different symmetry arguments have been used to prove wether a certain integral vanishes. All of them use the known symmetry of the system in order to prove that an integral is zero. These methods are explained in this section. In Section 3.1.2 they are used to obtain the target energy surface.

1. The first argument uses representation theory to prove whether the integrals are zero or not studying the direct product of the irreducible representations of the different terms that appear in them. The formal background of this method is explained in more detail in Ref. [48].

Given $\varphi^{(i)}$ and $\phi^{(i')}$ wave functions that transform as irreducible representations Γ_i and $\Gamma_{i'}$ respectively and an operator $O^{(j)}$ that transforms as Γ_j, the following integral can be considered:

$$o = \left\langle \varphi^{(i)} \middle| O^{(j)} \middle| \phi^{(i')} \right\rangle \tag{3.3}$$

Suppose now that the states $\varphi^{(i)}$ and $\phi^{(i')}$ are non degenerate[1]. Then under the effect of a symmetry operator $\hat{R}$ to either wave function or to the operator O, they transform as:

$$\hat{R}\varphi^{(i)} = \chi^{(i)}(R) \cdot \varphi^{(i)} \tag{3.4}$$

Where $\chi^{(i)}(R)$ is the character of the representation Γ_i for the operator $\hat{R}$, which is a scalar. Given an arbitrary symmetry operator $\hat{R}$, and taking into account that, as o is a scalar, then $\hat{R}o = o$, by applying the operator to both sides of equation (3.3), the following relation is obtained:

$$o = \hat{R}o = \hat{R}\left\langle \varphi^{(i)} \middle| O^{(j)} \middle| \phi^{(i')} \right\rangle = \left\langle \hat{R}\varphi^{(i)} \middle| \hat{R}O^{(j)} \middle| \hat{R}\phi^{(i')} \right\rangle = \chi^{(i)}(R) \cdot \chi^{(j)}(R) \cdot \chi^{(i')}(R) \cdot \left\langle \varphi^{(i)} \middle| O^{(j)} \middle| \phi^{(i')} \right\rangle \tag{3.5}$$

Which can be rewritten to give:

$$o = \chi^{(i)}(R) \cdot \chi^{(j)}(R) \cdot \chi^{(i')}(R) \cdot o \tag{3.6}$$

Therefore, as this is true for any symmetry operator $\hat{R}$, it must hold that $\chi^{(i)}(R)\chi^{(j)}(R)\chi^{(i')}(R) = 1$ regardless of the symmetry operator. This means that the direct product $\Gamma_i \otimes \Gamma_j \otimes \Gamma_{i'}$ must contain the fully symmetrical representation Γ_1 (sometimes written also as A_1). Therefore, using the character table and knowing which irreducible representation each term transforms as, some of the terms can be proven to be zero.

In fact, it can be shown that, even in the integrals where the direct product contains the fully symmetric representation, if the exact decomposition is known only the terms corresponding to the fully symmetric representation are non zero. This is why on top of the character tables it is useful to consider the coupling coefficient tables. Given a direct product $\Gamma_i \otimes \Gamma_j$ the coupling coefficient tables not only give what representations this direct product spans but also the coefficients of each representation in the direct product, the so called Clebsch-Gordan coefficients [49].

2. The second method is a particular case of the first one but it is worth mentioning as it can be easily applied without the need of character tables. The fact that this method does not need the use of character tables turns out to be very useful, as operating with character tables gets exponentially more complex the more terms are involved. This method is particular to the context of this work and, unlike the previous method, it is not completely general. This method uses the fact that the integrals in (3.2) are of the form:

$$E = \langle \Psi | \frac{\partial^k H}{\partial Q_{i_1} \cdots \partial Q_{i_n}} | \Psi \rangle \tag{3.7}$$

In this case, the product $\Psi\Psi$ is completely symmetric and thus the integral, from a representation stand point, only depends on the representations Γ_{i_j} of the coordinates Q_{i_j}. Taking now into account that the part of the representations Γ_{i_j} associated to translations of a direct lattice vector $\vec{r}$, as the most fundamental symmetry operation in a solid, can be identified through the coordinates $\vec{K_{i_j}}$ of a vector in the reciprocal space, the character of the representation Γ_{i_j} always takes the form:

$$\chi^{(i_j)} = e^{i\vec{K}_{i_j} \cdot \vec{r}} \tag{3.8}$$

As a consequence of this, with an analogous reasoning to the one used in the previous method, the integral 3.7 can be written as

[1] This is always true within the reach of this work but might not always be the case.

$$E = e^{i\vec{r}\cdot\vec{K}_{i_1}} \cdots e^{i\vec{r}\cdot\vec{K}_{i_n}} E = e^{i\vec{r}\cdot(\vec{K}_{i_1}+\cdots+\vec{K}_{i_n})} E \tag{3.9}$$

Where the product of the characters is only one when $\vec{K}_{i_1}+\cdots+\vec{K}_{i_n}$ corresponds to a point in the reciprocal lattice (i.e. has integer coordinates). For example, if all the Q_{i_j} transform as the reciprocal lattice vector $\vec{R} = (\frac{1}{2}, \frac{1}{2}, \frac{1}{2})$ then the integral is zero when an odd number of partial derivatives are taken. This is because if n is odd then $n\vec{R}$ does not have integer coordinates and thus is not a point of the reciprocal lattice forcing the integral to be zero.

3. The last method is another criterion that can be used without the need of character tables. This method is based on the fact that by applying a symmetry operator to the energy surface, the function must not change but the coordinates might change as a permutation of each other. This forces some of the terms to be zero as the energy function must stay invariant and said terms change from one form to another. This method, however, relies on having a geometrical understanding of the system and can be challenging to apply in some cases. Despite this, as for the scope of this work the system and the distortions are well known, this method can be easily applied.

To formalize the idea explained in the previous paragraph, let $E(Q_1, Q_2, ..., Q_n)$ be the energy surface of the system and P a symmetry operator of the cubic phase. Then the symmetry operator $\hat{P}$ transforms a certain coordinate Q_i into a new coordinate as the following transformation:

$$\hat{P}(Q_i) = \pm Q_{\rho(i)} \tag{3.10}$$

Where $\rho(i)$ is a permutation of the coordinates and the sign depends on the symmetry operator. The energy surface must be invariant under this transformation and thus:

$$E(Q_1, Q_2, ..., Q_n) = E(\hat{P}(Q_1), \hat{P}(Q_2), ..., \hat{P}(Q_n)) = E(\pm Q_{\rho(1)}, \pm Q_{\rho(2)}, ..., \pm Q_{\rho(n)}) \tag{3.11}$$

The simplest example of this method can be illustrated by supposing the symmetry operator $\hat{P}$ that leaves all coordinates but Q_1 invariant and transforms $Q_1 \mapsto -Q_1$. Then, applying P to the energy surface it is easy to see that all the terms that contain an odd power of Q_1 must be zero as the energy surface must be invariant under the transformation.

Another interesting example of the use of this method is considering the symmetry operator $\hat{P}$ that transforms $Q_1 \mapsto Q_2$ (and $Q_2 \mapsto Q_1$). This example illustrates the importance of the choice of the symmetry operator. In this case, in general, one cannot infer anything about the terms being zero or not. Imagine that the energy surface is given by:

$$E(Q_1, Q_2) = AQ_1^2 + BQ_2^2 + CQ_1Q_2 \tag{3.12}$$

Then applying the symmetry operator $\hat{P}$ the function stays invariant and thus nothing can be said about the coefficients A, B and C. However, if the energy surface is given by:

$$E(Q_1, Q_2, Q_3) = AQ_1^2 + BQ_2^2 + CQ_3^2 + DQ_1Q_3 \tag{3.13}$$

Applying the symmetry operator $\hat{P}$ shows that the coefficient D must be zero. These two examples show the importance of both choosing the right symmetry operator and applying it to the right energy surface. This is the reason why this method is the most useful after applying one or both of the other methods as the remaining energy surface is already somewhat reduced.

3.1.2 Obtaining the reduced energy surface

In order to simplify and reduce the energy surface given by equation (3.2), the steps followed have been the following; First, the problem has been split into three simpler problems. Supposing that the in-phase tilting, out-of-phase tilting and A-ion movements are independent, three independent energy surfaces can be obtained. Then, the full energy surface can be obtained by just taking into account the coupling between these distortions.

A quick analysis of how the distortions behave with respect to the different symmetry operators of the parent O_h group, show that both in-phase and out-of-phase tiltings transform as T_2 and the A-ion movement transforms as T_1. Furthermore, C.J.Howard and H.T.Stokes have shown that the tiltings of the octahedra have the representation $M_3^+ \otimes R_4^+$ where M_3^+ represents the in-phase tiltings and R_4^+ the out-of-phase tiltings (see Ref. [24]). This means that the in-phase distortions are related to the $\vec{M} = (\frac{1}{2}, \frac{1}{2}, 0)$ reciprocal space vector and the out-of-phase distortions to the vector $\vec{R} = (\frac{1}{2}, \frac{1}{2}, \frac{1}{2})$.

At this point some differences appear for the obtention of both energy surfaces associated to M and R phonon modes. For the out-of-phase tiltings, a similar argument as in Section 3.1.1 can be made to justify that the coefficients of the cubic terms must also be zero as $3\vec{R} = (\frac{3}{2}, \frac{3}{2}, \frac{3}{2})$ is not a reciprocal lattice point. However, for the in-phase tiltings as the reciprocal space vectors $(\frac{1}{2}, \frac{1}{2}, 0), (\frac{1}{2}, 0, \frac{1}{2}), (0, \frac{1}{2}, \frac{1}{2})$ are all equivalent, the cubic terms cannot be proven to be zero as the $Q_x Q_y Q_z$ term could be non vanishing.

This term involves a product of an odd number of coordinates that would make the energy surface depend on the particular sense (clockwise or anticlockwise) of rotation of the octahedra. We know that both directions are equivalent so this difference is not realistic. To solve this problem, the following argument is used. Using the coordinate system introduced in Fig. 3.1, consider the symmetry plane σ generated by the Z axis and the axis in the XY plane that is at an angle of 45 degrees with the X axis see figure 3.3.

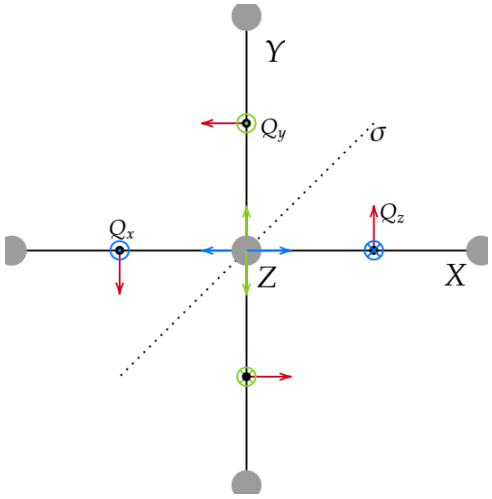

Figure 3.3: A representation of the Q_x, Q_y, Q_z tiltings and how these transform with a specific symmetry plane σ. The blue arrows represent the Q_x tiltings, the green arrows the Q_y tiltings and the red arrows the Q_z tiltings.

This symmetry operation transforms the coordinates as $\sigma((Q_x, Q_y, Q_z)) = (-Q_y, -Q_x, -Q_z)$. Given a natural number $n \in \mathbb{N}$, let's group all the terms of the energy surface that have combined powers of n as:

$$E_n = \sum_{i+j+k=n} A_{ijk} Q_x^i Q_y^j Q_z^k \tag{3.14}$$

As illustrated in the examples given in Section 3.1.1, and assuming that no extra information is known about the A_{ijk} terms, applying the symmetry operator σ to a generic even and odd term gives:

$$\sigma(E_{2n}) = E_{2n} \quad \text{and} \quad \sigma(E_{2n+1}) = -E_{2n+1}.$$

Since the energy surface must be invariant under the symmetry operation σ, it must hold that $E_{2n+1} = 0$ as $0 = E - \sigma(E) = \sum_{n\in\mathbb{N}} E_{2n+1}$ regardless of the coordinates $\{Q_x, Q_y, Q_z\}$. This means that all the odd terms in the energy surface must be zero.

Before continuing with the process a brief explanation of the notation used in the equations is given. The coordinates Q_{+i} and Q_{-i} represent the in-phase and out-of-phase tiltings respectively where the i index represents the spacial direction of the tilting. The coordinates Q_{ai} represent the A-ion movement in the i direction. These coordinates are directly related to the octahedral rotations and to the A-ion displacements and they are further discussed in Section 3.3.2 where the tilting coordinates $Q_{\pm i}$ are defined in Figure 3.8 and the A-ion coordinates are just the displacements of ion with respect to the cubic phase. However, for this section, the only important thing is that the coordinates Q_{+i} and Q_{-i} transform as T_2 and the coordinates Q_{ai} transform as T_1.

Now that some of the terms have been proven to be zero, the next step is to get the exact reduced form using the first method explained in Section 3.1.1. As discussed previously in this section, the in-phase and out-of-phase tiltings have the representations M_3^+ and R_4^+ respectively and they both transform as T_2. Therefore, the second order terms are obtained just by analyzing the coupling coefficients of the direct product $T_2 \otimes T_2$ that span the completely symmetric representation. For the fourth order terms however, the process is a bit more complex. The direct product $T_2 \otimes T_2$ gives a combination $T_1 + T_2 + A_1 + E$. Now, the direct product of all of those terms by T_2 must be calculated which will in terms give a certain combination $A_1 + T_1 + E + T_2 + A_2$. Lastly, the product of all of those terms by T_2 must be calculated in order to determine the exact form of the terms contained in A_1. However, this process can be slightly simplified by noticing that the only term from $T_2 \otimes T_2 \otimes T_2$ that gives A_1 when multiplied by T_2 is the term T_2. This means that only some of the calculations need to be done (see figure 3.4).

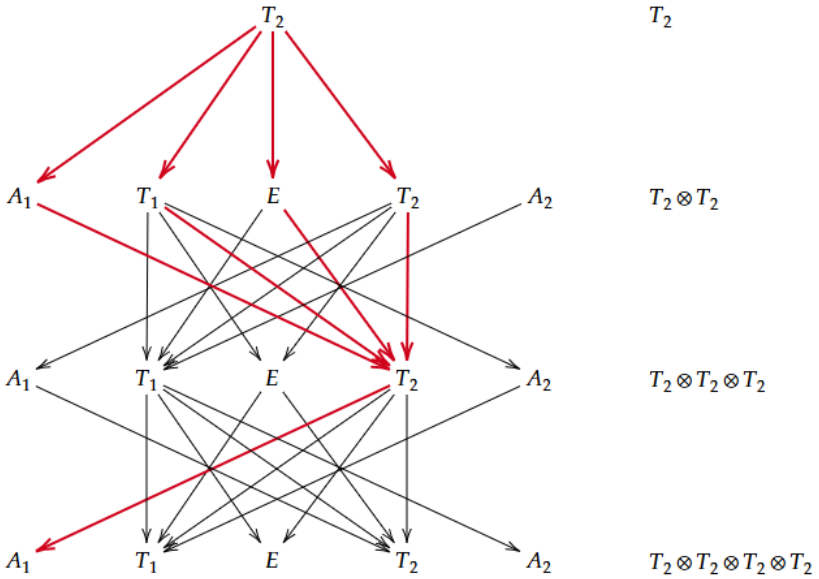

Figure 3.4: A schematic representation of the different irreducible representations that form the product $T_2 \otimes T_2 \otimes T_2 \otimes T_2$. The arrows in red are the only ones for which the coupling coefficients have to be calculated.

The process described here for the octahedral tiltings is the same for the A-ion movement. The only difference is that the A-ion movement transforms as T_1 and thus the direct product $T_1 \otimes T_1$ gives a different combination of irreducible representations. The process is exactly the same and thus the final result is similar to the one obtained for the octahedral tiltings. The three independent energy surfaces thus are:

$$E_+ = E_0 + K_+(Q_{+x}^2 + Q_{+y}^2 + Q_{+z}^2) + I_{++}(Q_{+x}^4 + Q_{+y}^4 + Q_{+z}^4) + H_{++}(Q_{+x}^2Q_{+y}^2 + Q_{+x}^2Q_{+z}^2 + Q_{+y}^2Q_{+z}^2) \quad (3.15)$$

$$E_- = E_0 + K_-(Q_{-x}^2 + Q_{-y}^2 + Q_{-z}^2) + I_{--}(Q_{-x}^4 + Q_{-y}^4 + Q_{-z}^4) + H_{--}(Q_{-x}^2Q_{-y}^2 + Q_{-x}^2Q_{-z}^2 + Q_{-y}^2Q_{-z}^2) \quad (3.16)$$

$$E_a = E_0 + K_a(Q_{ax}^2 + Q_{ay}^2 + Q_{az}^2) + I_{aa}(Q_{ax}^4 + Q_{ay}^4 + Q_{az}^4) + H_{aa}(Q_{ax}^2Q_{ay}^2 + Q_{ax}^2Q_{az}^2 + Q_{ay}^2Q_{az}^2) \quad (3.17)$$

To study the mixing between in-phase and out-of-phase tiltings one must now take into account terms involving the cross-coupling terms involving both Q_{+i} and Q_{-i} coordinates. The process is exactly the same as before and thus the final result is similar to the one obtained for the purely in-phase or out-of-phase octahedral tiltings. The only difference is that the in-phase and out-of-phase tiltings are now coupled. The energy surface can be written as:

$$E_T = E_0 + \sum_{j=\pm} K_j(Q_{jx}^2 + Q_{jy}^2 + Q_{jz}^2) + \sum_{j,k=\pm} I_{jk}(Q_{jx}^2Q_{kx}^2 + Q_{jy}^2Q_{ky}^2 + Q_{jz}^2Q_{kz}^2) + \sum_{j,k=\pm} H_{jk}(Q_{jx}^2Q_{ky}^2 + Q_{jx}^2Q_{kz}^2 + Q_{jy}^2Q_{kz}^2) \quad (3.18)$$

The coefficients are chosen in a way where K_j represents the quadratic terms, I_{jk} is the coefficient multiplying the quartic terms where no spacial coordinates are mixed within the same term (for example $Q_{+x}^2Q_{ax}^2$ or $Q_{-y}^2Q_{-y} = Q_{-y}^4$). Lastly, H_{jk} is the coefficient multiplying the quartic terms where the spacial coordinates are mixed (for example $Q_{+x}^2Q_{+y}^2$ or $Q_{+y}^2Q_{-z}$). Here, $I_{jk} = I_{kj}$ and $H_{jk} = H_{kj}$. On top of that, since, by hypothesis the same coordinate cannot have a + and − tilting at once the term I_{+-} is zero as terms such as $Q_{+x}^2Q_{-x}^2$ must be zero.

By using analogous arguments, the terms that mix the A-ion movement with the tiltings can be studied. The only difference being that the A-ion movement transforms as T_1 and thus the direct product $T_1 \otimes T_2$ gives a different combination of irreducible representations. In this case, the process is exactly the same and thus the final result is similar to the one obtained for the octahedral tiltings. The expression however, is somewhat more complex and it is therefore useful to define the following notation:

$$\Delta_{jk}(\{Q_i\}) = Q_{jx}^2Q_{kx}^2 + Q_{jy}^2Q_{ky}^2 + Q_{jz}^2Q_{kz}^2 \quad (3.19)$$

$$\Xi_{jk}(\{Q_i\}) = Q_{jx}^2Q_{ky}^2 + Q_{jx}^2Q_{kz}^2 + Q_{jy}^2Q_{kx}^2 + Q_{jy}^2Q_{kz}^2 + Q_{jz}^2Q_{kx}^2 + Q_{jz}^2Q_{ky}^2 \quad (3.20)$$

It is worth noting that the term $\Delta_{jk}(\{Q_i\})$ has the same form as the one following the I_{jk} coefficients in the previous section. In fact, given that a coordinate cannot have two distinct tilting modes at once (i.e. if $Q_{+x} \neq 0$ then $Q_{-x} = 0$), the term $\Xi_{jk}(\{Q_i\})$ is also the same as the one that follows the H_{jk} coefficients in the previous section. With this notation, the energy surface can be written as:

$$E = E_0 + \sum_j K_j(Q_{jx}^2 + Q_{jy}^2 + Q_{jz}^2) + \sum_{j,k} I_{jk}\Delta_{jk}(\{Q_i\}) + \sum_{j,k} H_{jk}\Xi_{jk}(\{Q_i\}) \quad (3.21)$$

Where the subindices now run over the set $\{+, -, a\}$ and, as before, $I_{jk} = I_{kj}$ and $H_{jk} = H_{kj}$. On top of that, the term I_{+-} is still zero. However, the movement of the A-ion can be in the same direction as one of the tilting axis and thus the terms I_{+a} or I_{-a} can exist.

3.2 Study of the energy parameters

Once the general form of the reduced energy surface is known, the next step is to interpret the physical meaning of the different parameters as well as to obtain conditions on the values of the coefficients that if met the lowest energy phase can be identified. Lastly, it is interesting to obtain the real values of some of the parameters in order to understand the tendencies that occur in experimental systems.

This section is divided into two parts:

1. **Physical interpretation of the parameters:** In this part the physical meaning of the coefficients in equation 3.21 is explained. The coefficients are interpreted in terms of the energy cost of a certain distortion.
2. **Conditions for the stable phase:** In this part, relations between the coefficients are obtained and the connection between these relations and the stable phases is explained.

3.2.1 Physical interpretation of the parameters

In order to understand the physical meaning behind the coefficients of the energy surface, it is easier to first consider the simpler case of the octahedral tiltings described by the equation (3.18). However, regardless on having the simpler case or the more complex one, the coefficients are associated to the energy cost of a certain distortion. Keep in mind however that despite the word "cost" being used this value can be positive or negative. If a given coefficient is large in absolute value, then the system will tend to avoid the distortion associated to that coefficient if it is positive and will tend to favor the distortion if it is negative. However, the values of the coefficients are not enough to determine the stable phase as the different modes are coupled and thus the same distortion can multiply both positive and negative coefficients making the system tend to a balance.

In order to understand the meaning of the coefficients in equation (3.18), it can be useful to rewrite the equation as a function of (3.15) and (3.16). This makes it easier to unwrap the meaning of the coefficients. The equation can be rewritten as:

$$E_T(\{Q_i\}) = -E_0 + E_+(\{Q_i\}) + E_-(\{Q_i\}) + H_{+-}(Q_{+x}^2 Q_{-y}^2 + Q_{+x}^2 Q_{-z}^2 + Q_{+y}^2 Q_{-z}^2) \tag{3.22}$$

This equation shows that the energy can be written as two independent functions, one associated to the in-phase tiltings one associated with the out-of-phase tiltings while the H_{+-} term is the energy cost of having both in-phase and out-of-phase tiltings at the same time. This is a reasonable assumption as the H_{+-} term is the only one that couples both types of tiltings. In order to understand the meaning of the K_j, I_{jj} and H_{jj} terms, it is useful to study specific cases and analyze how the $E_+(\{Q_i\})$ and $E_-(\{Q_i\})$ simple surfaces behave. Since the simple surfaces for in-phase and out-of-phase tiltings are the same, the next part of the work focuses only on the in-phase surface. However the exact same methods can be applied for the out-of-phase one. If the octahedra are tilted in only one axis, say the x axis, then the simple energy surface is given by:

$$E_+(\{Q_i\}) = E_0 + K_+(Q_{+x}^2) + I_{++}(Q_{+x}^4) \tag{3.23}$$

However, if tiltings along two or more axes are allowed, the energy surface takes the general form of equation (3.15). Therefore, it can be deduced that the H_{++} term is associated to the energy cost of having more than one in-phase tilting at the same time. Finally, since near the cubic phase ($Q_i = 0$) the K terms are the ones with the most influence, they can be interpreted as the responsables for having any tiltings at all. Since the cubic phase is generally unstable, the K terms are expected to be negative. In fact, in Subsection 3.3.3, it will be seen that this is the case for most of our experimental systems (see Tab. 3.10). With this

in mind, the I terms can be interpreted as the energy stabilization terms. This means that the I terms are expected to be positive as they are the ones that stabilize the system (see figure 3.5).

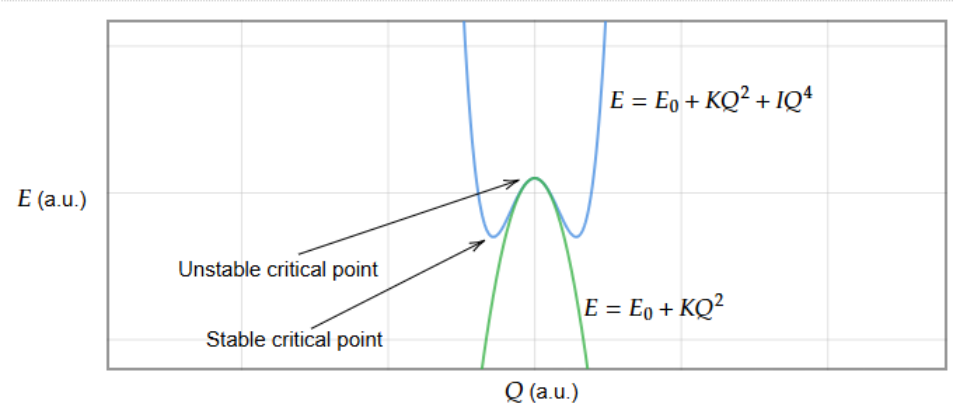

Figure 3.5: A qualitative graph to visualize the importance of the I coefficients. The scale in this graph is not accurate as it is intended to only portray the behavior of the function. The X axis represents the distortion Q and the Y axis represents the energy E. Both the energy and the distortions are given in arbitrary units.

One can now see the reason behind the labeling of the different coefficient by different letters.

- The K **coefficients** are called the force constants and they model the destabilization of the system around the cubic phase.
- The I **coefficients** are the terms that model the stabilization of the system.
- The H **coefficients** are the ones that model the coupling between different tilting modes whether this is between the same type of tilting or between the in-phase and out-of-phase tiltings.

When the A-ion is added to the system, see (3.21), the interpretation of the coefficients is a little bit different. One could once again separate the equation into purely tilting terms and A-ion terms. The surface would then be written as:

$$E(\{Q_i\}) = -2E_0 + E_T(\{Q_i\}) + E_a(\{Q_i\}) + I_{a+}\Delta(\{Q_i\}) + I_{a-}\Delta(\{Q_i\}) + H_{a+}\Xi(\{Q_i\}) + H_{a-}\Xi(\{Q_i\}) \tag{3.24}$$

The interpretation of the coefficients regarding the A-ion movement is the following:

- The I_{aj} **coefficients** correspond to the energy cost of moving the A-ion in the direction of the axis of a tilting.
- The H_{aj} **coefficients** are associated to the energy cost of moving the A-ion in a direction that is not aligned with the tilting axis.
- The K_a, I_{aa} **and** H_{aa} **coefficients** correspond to the destabilization, stabilization and the coupling between the A-ion movements in the three different axes respectively.

3.2.2 Relations between the coefficients and phase diagrams

This subsection is dedicated to the interpretation of the model and the study on the importance of the different coefficients in determining the most stable phase of the system. In this section, some conditions

on the coefficients will be deduced that relate to the stability of the different phases. Later in Section 3.4, these conditions will be compared with the results obtained from the numerical simulations.

Pure tiltings:

Similarly to the approach taken in Subsection 3.2.1, the relations between the coefficients can first be studied supposing that the octahedra are only tilted with in-phase tiltings. Since the energy surfaces for the in-phase and out-of-phase tiltings are the same, the analysis can be done for either of them and instantly extended to the other. The subindices in the coefficients corresponding to the in-phase tiltings are dropped as it is understood by context that this is the phase worked on. Consider now a simple case where $H = 0$. In this case, the energy surface can be written as:

$$E = E_0 + K(Q_x^2 + Q_y^2 + Q_z^2) + I(Q_x^4 + Q_y^4 + Q_z^4) = E_0 + f_x(Q_x) + f_y(Q_y) + f_z(Q_z) \tag{3.25}$$

Where the functions f_i are given by:

$$f_i(Q_i) = K(Q_i^2) + I(Q_i^4) \tag{3.26}$$

The minimum for the energy surface is then given by the three independent minima of one variable functions f_i $(i = x, y, z)$ and since the coefficients are all the same, in the minimum configuration corresponds with $Q_x = Q_y = Q_z$. With this notation, it is possible to rewrite the energy surfaces in equations (3.15) and (3.16) as:

$$E = E_0 + f_x(Q_x) + f_y(Q_y) + f_z(Q_z) + H(Q_x^2Q_y^2 + Q_x^2Q_z^2 + Q_y^2Q_z^2) \tag{3.27}$$

This way of writing the functions gives an important idea about the distortions; *No matter the number of distortions, their magnitude will always be the same* (i.e. the minimum involves rotations of the same magnitude in 1, 2 or 3 axes). This holds because the term multiplying the H does not have a "preference" for any of the coordinates and since neither do the f_i functions, the system as a whole will not have a preference for any of the coordinates. This means that if more than one distortion is present they will all be of the same magnitude.

The problem now is to determine the relations between the K, I and H that dictate whether the system stabilizes in one, two or three distortions. Before starting the rigorous analysis, some qualitative information can be deduced from the known geometric shape of the energy surface. Just as in the $\mathbb{R}^3$ euclidean space, the square of the distance to the origin of a certain distortion configuration can be given by:

$$d^2 = Q_x^2 + Q_y^2 + Q_z^2 \tag{3.28}$$

Which is exactly the term following the K coefficient. Now, noting that the distance to the 4^{th} power takes the form:

$$d^4 = Q_x^4 + Q_y^4 + Q_z^4 + 2(Q_x^2Q_y^2 + Q_x^2Q_z^2 + Q_y^2Q_z^2). \tag{3.29}$$

Looking at the equations (3.15) and (3.16), it can be seen that when the condition $H = 2I$ is satisfied, the energy surface only depends on the distance to the origin as

$$E(d) = E_0 + Kd^2 + Id^4. \tag{3.30}$$

This means that, at this configuration, the system will have the same energy in a $(a00)$ state with $Q_x = Q$, in a $(aa0)$ state with $Q_x = Q_y = Q/\sqrt{2}$ or in a (aaa) state with $Q_x = Q_y = Q_z = Q/\sqrt{3}$. This means that exactly at this configuration of $H = 2I$, the system could be in either phase. This is thus a likely candidate line that conditions phase stability. This reasoning also shows qualitatively that the effect of K over phase stability is not important, as the term following K is always spherically symmetric (i.e. it only depends on the distance).

On top of this, by looking at equation (3.27), it can be inferred that if $H < 0$ then the system will tend to present all three distortions at the same time and thus tend to stabilize in the (aaa) phase. However, if H is positive and very large compared to the other coefficients, the system will tend to minimize the term following H and thus will tend to have only one distortion at a time. The interesting question now is to determine whether there is a certain combination of coefficients around $H \sim 2I$ where the $(aa0)$ phase is favored.

Once some intuition on the expected results is obtained, the next step is to study the system in a more rigorous way. The first step is to obtain the extrema of the energy surface. This problem can be simplified by the previously mentioned fact that the magnitude of all the distortions is the same. This means that the extrema of the energy surface will only appear within the line with directing vector $v_1 = (1, 0, 0)$ if the system is in the $(a00)$ phase, within the line with directing vector $v_2 = (1, 1, 0)$ if the system is in the $(aa0)$ phase and within the line with directing vector $v_3 = (1, 1, 1)$ if the system is in the (aaa) phase. The equation for the energy within these lines can be written as:

$$\begin{aligned} (a00): &\quad E_1 = E_0 - KQ_1^2 + IQ_1^4 \\ (aa0): &\quad E_2 = E_0 - 2KQ_2^2 + 2IQ_2^4 + HQ_2^4 \\ (aaa): &\quad E_3 = E_0 - 3KQ_3^2 + 3IQ_3^4 + 3HQ_3^4 \end{aligned} \tag{3.31}$$

Where E_i represents the energy for the phase with i tiltings and $Q_i = Q_x = Q_y = Q_z$ represents the general coordinate of distortion corresponding to the directing vector v_i. It is also worth noting that for the following reasoning the letters K, I and H represent the magnitude of the coefficients so the minus sign for K has been explicitly included in the definition of the energy. The coefficient I stabilizes the system and must thus be positive and the coefficient H has been taken positive since it is known that when this is negative the system favours the phase (aaa). In Subsection 3.3.3 it will be seen that the signs of the coefficients for a real system in fact coincide with these. With this in mind, by taking the derivative of the energy with respect to the coordinates Q_i and setting it to zero, the coordinates at the extrema of the energy functions can be obtained. It is worth noting that, as expected, the trivial maximum at $Q_i = 0$ is present in all three cases but this will be ignored. The nontrivial minimum coordinates and their corresponding energies are:

$$\begin{aligned} Q_1 &= \pm\sqrt{\frac{K}{2I}} &&\Rightarrow\ E_1 = -\frac{K^2}{4I} \\ Q_2 &= \pm\sqrt{\frac{K}{2I+H}} &&\Rightarrow\ E_2 = -\frac{K^2}{2I+H} \\ Q_3 &= \pm\sqrt{\frac{K}{2I+2H}} &&\Rightarrow\ E_3 = -\frac{3K^2}{4I+4H} \end{aligned} \tag{3.32}$$

Studying now the conditions over the coefficients that must be satisfied in order for one phase to be favored over the other (i.e. one energy to be lower than the other), it can be seen that the conditions are:

$$\begin{aligned} &E_1 < E_2 \Leftrightarrow H > 2I \\ &E_2 < E_3 \Leftrightarrow H > 2I \\ &E_1 < E_3 \Leftrightarrow H > 2I \end{aligned} \tag{3.33}$$

This is congruent with the previous qualitative reasoning as it shows that $H = 2I$ is a line that determines phase stability. Furthermore, by analyzing the energy favoured at both sides of the line $H = 2I$, it can be seen that the (aaa) phase is favoured when $H < 2I$ and the $(a00)$ phase is favoured when $H > 2I$. However, the most important result is that the $(aa0)$ phase is never favoured (only exactly over the $H = 2I$ line). This means that the system will always tend to have either one or three distortions at the same time. See figure 3.6 for a visual representation of the phase diagram.

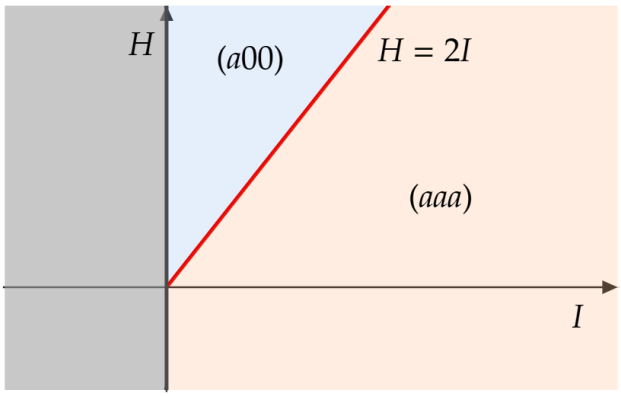

Figure 3.6: This figure shows the phase diagram obtained from the inequalities in equation (3.33). The section in blue represents the systems that stabilize in the $(a00)$ phase and the section in orange the systems that stabilize in the (aaa) phase. The section in gray represents the section with a negative value for I which is of no physical interest.

So far, the analysis has been done for pure tiltings only. However, real systems are more complex as they can present A-ion movements as well as mixed tiltings. In the rest of the subsection, the analysis for pure tiltings will be used as a base to analyze the coupled systems.

Mixed tiltings ($Pnma$):

A central part of this work is the analysis of the $Pnma$ phase as this phase is the most common phase in real systems. The approach used to analyze this phase can be generalized to other mixed tilt systems but will be explained here in particular for $Pnma$.

The approach is simple, looking at Howard and Stokes's table (see Fig. 3.2), there is two distinct "paths" to $Pnma$ from the cubic $Rm\bar{3}m$ phase:

$$\begin{aligned}(c^0c^0c^0) \rightarrow (a^+c^0c^0) \rightarrow (a^+b^-b^-)\\ (c^0c^0c^0) \rightarrow (c^0b^-b^-) \rightarrow (a^+b^-b^-)\end{aligned} \tag{3.34}$$

The first transition within each path is the one already studied while the second one can be analyzed by taking the energy of the first transition and adding the energy corresponding to adding two b^- tiltings in the first case or one a^+ tilting in the second. Therefore, the energy surface for $(a^+b^-b^-)$ can be written as:

$$\begin{aligned}E_1(a^+b^-b^-) = E(c^0c^0a^+) + (2H_{+-}Q_a^2 - 2K_-)Q_b^2 + I_{--}Q_b^4\\ E_2(a^+b^-b^-) = E(c^0b^-b^-) + (2H_{+-}Q_b^2 - K_+)Q_a^2 + I_{++}Q_a^4\end{aligned} \tag{3.35}$$

Supposing that during the transition the distortion Q_a stays constant in the first case and Q_b stays constant in the second, the energy can be understood as a polynomial in the variable Q_b or Q_a respectively. Note that this is an approximation. For instance, for $NaTaO_3$, both distortions change from $P4/mbm$ to $Pnma$ and from $Imma$ to $Pnma$ (see Table 3.4).

Once the approximation is made, the energy for the $(a^+b^-b^-)$ is only lower than the energy for the parent $(c^0c^0a^+)$ or $(c^0b^-b^-)$ phases if the following conditions are satisfied:

$$\begin{aligned}(a^+c^0c^0) \rightarrow (a^+b^-b^-) : (2H_{+-}Q_a^2 - 2K_-) < 0\\ (c^0b^-b^-) \rightarrow (a^+b^-b^-) : (2H_{+-}Q_b^2 - K_+) < 0\end{aligned} \tag{3.36}$$

If the conditions are satisfied, then by setting the derivative of the energy with respect to Q_a or Q_b to zero, the coordinates of the minimum can be obtained. By substituting the coordinates of the minimum, the

difference in energy between the $(a^+b^-b^-)$ and the parent phases can be obtained and it is given by:

$$\begin{aligned}(a^+c^0c^0) \rightarrow (a^+b^-b^-) &: \frac{(2H_{+-}Q_a^2 - 2K_-)^2}{4I_{--}} \\ (c^0b^-b^-) \rightarrow (a^+b^-b^-) &: \frac{(2H_{+-}Q_b^2 - K_+)^2}{4I_{++}}\end{aligned} \tag{3.37}$$

Equations (3.36) and (3.37) show that the stability of the mixed tilting phase $Pnma$ strongly depends on H_{+-} as the lower this term the more stable the phase is.

Movement of the A-ion:

The movement of the A-ion is restricted to some of the tilt systems (see Fig. 3.2). In fact, out of all the pure tilt systems only the out-of-phase $(aa0)$ tilting (i.e. $Imma$ or $(a^0b^-b^-)$) allows for the movement of the A-ion. Since the movement of the A-ion gives more degrees of freedom to the system, it is expected that it will lower the energy of the system. In fact in Subsection 3.3.3 it will be seen that the energy of the system is lower when the A-ion movement is considered.

Taking this into account, since in the $H = 2I$ line the system accepts $(a00)$, $(aa0)$ and (aaa), the addition of the A-ion movement will allow for the stabilization of the out-of-phase $(aa0)$ tilting. If the A-ion lowers the energy of the system enough, for some values of the coefficients such that $H \approx 2I$ the system will still stabilize in $(aa0)$ despite the system not being exactly at the $H = 2I$, line. This can be understood as the A-ion movement forcing a new region to appear in the phase diagram in Figure 3.6 where the $(aa0)$ phase is stable. This is shown in Figure 3.7.

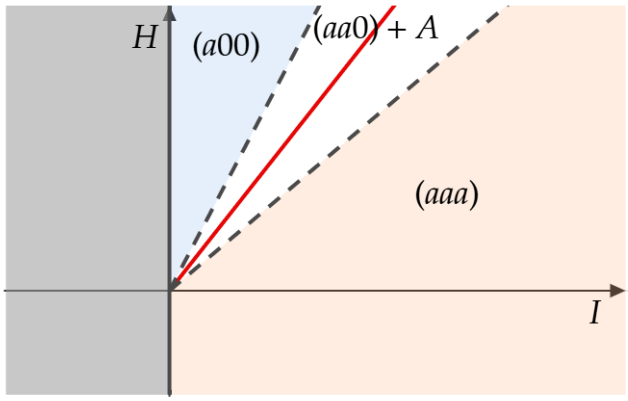

Figure 3.7: This diagram shows how the diagram in Figure 3.6 changes when the movement of A is considered. This is a qualitative phase diagram as the exact analytic expressions for the changes in-phase haven't been obtained. It is worth noting that when the movement of A is considered the phase space gets more complex and higher dimensional, this figure is only a representation of what adding the extra complexity would do to the existing model.

The main conclusions of this subsection can be summarized as follows:

- When only considering pure in-phase or out-of-phase tiltings, **the line $H = 2I$ determines the phase stability of the system** as shown in Figure 3.6.
- When considering mixed tiltings, **the stability of the $Pnma$ phase depends on the H_{+-} coefficient** as shown in equations (3.36) and (3.37).
- The movement of **the A-ion allows for the stabilization of two tilting modes** as seen in Figure 3.7.

3.3 Results of the simulations and obtention of the parameters

This section is divided into three parts. First, the methodology used to extract the information from the simulations is explained. This is done in Subsection 3.3.2. Then, in Subsection 3.3.2, the geometry of the different phases is studied and the distortion coordinates are extracted. Finally, in Subsection 3.3.3, the coefficients of the energy surface are obtained and analyzed.

3.3.1 Extracting results from the simulations

In this part of the work, the general process of obtaining the geometry and the parameters of the different configurations is explained. This process is the same regardless of the chemical configuration of the system.

As noted in the introduction of this section, the first step is to identify the coordinates of the distorted systems given by the tables in [23]. The tables in this paper show the spacial coordinates of the different atoms in the primitive cell. For some of the atoms, one or more of the spacial coordinates are given as an unknown variable approximated to a certain value. This means that these coordinates are the ones that explain the distortion of the system and may vary depending on the chemical configuration.

In order to simulate the system using CRYSTAL [45], an approximate value is chosen for the unknown coordinates and all the coordinates are introduced in the input file. Then, the space group symmetry is inputted. The specification of the group ensures that all the iterative steps in the simulation are forced to maintain the symmetry and thus, the output will be the configuration with the lowest energy within the symmetry constraints. This holds because the forces acting on the system follow the same symmetries as the system itself. Therefore, as the program simulates the evolution of the system by means of the forces acting on it, the system will maintain the chosen symmetry at all times. For instance, if the $Imma$ phase is chosen, all the iterative steps will maintain the $Imma$ symmetry. This means that the output will be the configuration with the lowest energy within the $Imma$ symmetry constraints.

The program outputs all the information of the final relaxed state of the crystal as well as some information about the in between steps such as the energy or the geometry. In particular, the program outputs a set of coordinates for the atoms in the least-energy configuration within the constraints. Unlike the input coordinates, these are not given as a function of the unknown variables and these coordinates are adjusted to the values that minimize the energy of the system. The output file also contains the minimum energy of the system. The coordinates of the atoms are then introduced into the crystal visualization software VESTA [8] in order to represent the system. This visualization software allows a precise and easy way to measure the angles and distances between the atoms in the system. The angles and distances are then used to calculate the parameters of the energy surface.

With a way to easily visualize the system, the next step is to choose a suitable set of distortion coordinates that correctly measure the tiltings. To illustrate the choice of coordinates, the simpler case of the $(a00)$ is used. Remember that this phase is a simple tilting of the octahedra along the X axis (see Fig. 3.1 for the choice of coordinates). The X anions along the Y and Z axes are thus displaced within the line of equidistance between the B cations. Here, it is natural to choose the displacement of the X anions as the distortion coordinates as this distance is zero when no distortion is present and grows as the distortion increases. To generalize this to the case with mixed tiltings, the distortion coordinate Q_{x_i} is defined as the projection of the displacement of the X anion into the plane formed by the other two coordinates. A geometric representation of this is shown in figure 3.8.

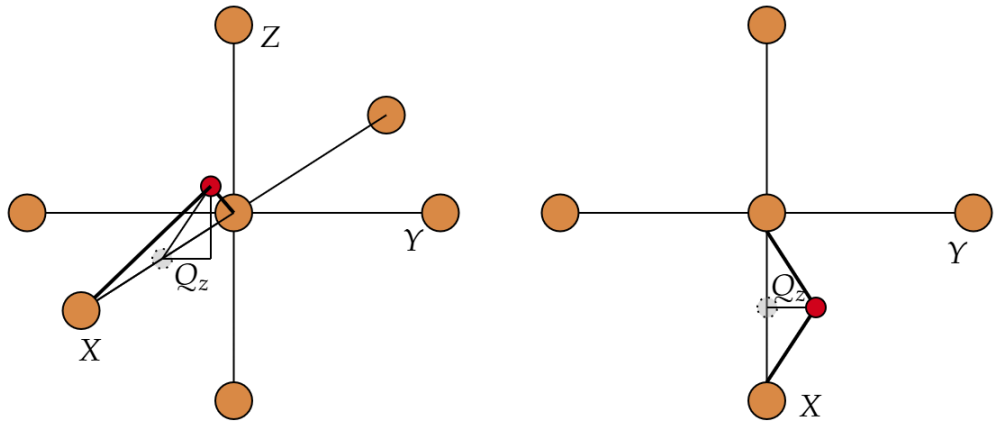

Figure 3.8: This figure shows a representation of the election of the Q_z coordinate. In the left figure one can see the three dimensional structure of the crystal where the atoms in orange represent the B cations and the atom in red represents the X anion. In the right figure the projection into the XY plane is shown. In both figures the grey dotted circle represents the original position of the X anion in the cubic phase.

As it was introduced before, VESTA allows to measure the angles and distances between the atoms and thus the distortion coordinates can be calculated by straightforward but somewhat lengthy trigonometric equations. The measurement of the angles and distances are also used to justify the fact that the octahedral deformations can be neglected (see Subsection 3.3.2). Given that each phase allows many possible distortions (see Ref [23]) this often requires a detailed analysis of the particular geometry of the system to extract the corresponding rotation angles and coordinates.

Once the distortion coordinates and the energy of the system are known for the minimum energy configuration in each phase, the next step is to calculate the coefficients of the energy surface. To do this, a similar approach to the one used in section 3.2.2 is used. This approach uses the fact that the energy surface is the simplest when the system does not have any mixed "+" and "-" tiltings. This means that by studying the system only in the $P4/mbm$, $I4/mcm$ and $Im\bar{3}$ phases (i.e. the $(a^+a^0a^0)$, $(a^+a^+a^0)$ and $(a^+a^+a^+)$ phases respectively) the coefficients can be calculated by solving a simple linear system of equations. It is possible to rewrite the energy surfaces given in equation (3.31) as:

$$\begin{aligned} E_{P4/mbm} &= E_0 + K_+(Q_{+1}^2) + I_{++}(Q_{+1}^4) \\ E_{I4/mcm} &= E_0 + 2K_+(Q_{+2}^2) + 2I_{++}(Q_{+2}^4) + H_{++}(Q_{+2}^4) \\ E_{Im\bar{3}} &= E_0 + 3K_+(Q_{+3}^2) + 3I_{++}(Q_{+3}^4) + 3H_{++}(Q_{+3}^4) \end{aligned} \tag{3.38}$$

where the $\{1, 2, 3\}$ subindices in the coordinates indicate that the point of stabilization is different for the different phases. Given that the coordinates Q_{+j}, the energies E_i and the energy of the cubic phase E_0 are known quantities, the set of equations can be solved for the coefficients K_+, I_{++} and H_{++}. In fact, the equations can be rewritten as:

$$\begin{pmatrix} Q_{+1}^2 & Q_{+1}^4 & 0 \\ 2Q_{+2}^2 & 2Q_{+2}^4 & Q_{+2}^4 \\ 3Q_{+3}^2 & 3Q_{+3}^4 & 3Q_{+3}^4 \end{pmatrix} \begin{pmatrix} K_+ \\ I_{++} \\ H_{++} \end{pmatrix} = \begin{pmatrix} E_{P4/mbm} - E_0 \\ E_{I4/mcm} - E_0 \\ E_{Im\bar{3}} - E_0 \end{pmatrix} \tag{3.39}$$

where the system of equations is now in the form $Ax = b$ with a known matrix A and a known vector b. This system of equations can be solved using the standard methods for solving linear systems. The solution

of this system gives the coefficients K_+, I_{++} and H_{++}. The same process can be repeated for the out-of-phase tiltings in order to obtain the coefficients K_-, I_{--} and H_{--}. The only difference is that the phases analyzed have to be the $I4/mcm$, $Imma$ and $R\bar{3}c$ phases (i.e. the $(a^-a^0a^0)$, $(a^-a^-a^0)$ and $(a^-a^-a^-)$ phases respectively). However, a problem arises when studying the $Imma$ phase as this phase presents freedom of movement in the A-ion. To solve this, the simulation is executed with the added constraint of the A-ion being fixed in place. This yields a new $Imma'$ phase that does not depend on the movement of A. With this method the set $\{K_+, K_-, I_{++}, I_{--}, H_{++}, H_{--}\}$ of coefficients is obtained.

In order to obtain the H_{+-} coefficient, a phase has to be chosen where both in-phase and out-of-phase tiltings are present. In order to correctly account for this coupling we need to avoid accounting for the A-ion movement. In this case, the energy surface can be simply written as:

$$E = E_0 + K_+(Q_+^2) + K_-(Q_-^2) + I_{++}(Q_+^4) + I_{--}(Q_-^4) + H_{++}(Q_+^4) + H_{--}(Q_+^4) + H_{+-}(Q_+^2Q_-^2) \quad (3.40)$$

with the addition of some constants depending on the amount of "+" and "-" tiltings. The problem arises when trying to find said phase as, according to Woodward [23], all of the phases that present both in-phase and out-of-phase tiltings also present A-ion movement. And, as it will be shown in Subsection 3.3.2, the quantitative study of the movement of the A-ion is beyond the scope of this work. However, thanks to the software CRYSTAL, it is possible to fix in place the A-ion and simulate the system with this added constraint. This process yields a set of coordinates and an energy for the system that differ from the ones obtained when the A-ion is free to move and must be treated as a different phase. With this tool, the phase $Pnma'$ has been chosen as the one with both in-phase and out-of-phase tiltings. The $'$ next to $Pnma$ is written to clarify that this is the $Pnma$ phase with the added constraint of fixed A-ions, same as in the case of $Imma'$. The energy surface can be written as:

$$E_{Pnma'} = E_0 + K_+(Q_+^2) + 2K_-(Q_-^2) + I_{++}(Q_+^4) + 2I_{--}(Q_-^4) + H_{--}(Q_-^4) + H_{+-}(Q_+^2Q_-^2) \quad (3.41)$$

where all the values and coefficients are known and the only unknown is H_{+-}. This way one can simply solve for H_{+-} to obtain the last coefficient.

3.3.2 Numerical results of the simulations: geometry

The results of the simulations can be separated into two parts. The first part is the geometry of the stabilized systems without taking into account the energy. Once the geometry is known, the second part is to obtain the coefficients of the energy surface using the values of the geometry and the energies of the phases.

This section is dedicated to the geometry of the systems. First, the geometries of the octahedra are studied. Once the geometries of the octahedra are known, the tilting coordinates are studied. This coordinates will later be used to obtain the coefficients of the energy surface.

Octahedral deformations:

The following tables show the octahedral lengths and inner angles for the different phases studied for the compounds $NaTaO_3$, $LaAlO_3$ and $SrTiO_3$. The octahedral lengths are the distances between the B cation and the X anions in the three different axes. The inner angle ϕ_z is defined as the smallest angle formed by the X and Y axis. The same definition is used for the angles ϕ_x and ϕ_y (see Figure 3.9). These parameters fully describe the octahedral deformations. If the octahedra are not deformed it is expected to obtain the same length regardless of the direction and three angles of 90 degrees.

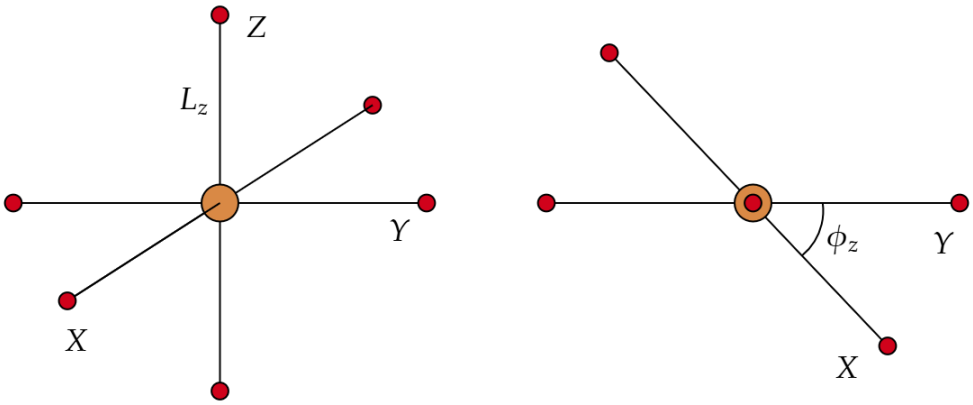

Figure 3.9: This figure shows how the octahedral lengths L_i and the inner angles ϕ_i are defined. The left hand figure shows a 3D view of the octahedron while the right hand figure shows a view of the octahedron from the Z axis. The orange ball represents the B cation and the red balls represent the X anions.

Before showing any numerical results, it is worth noting that the x, y and z labels are arbitrary and any permutation of the labels is valid as long as it is coherent. This labels are used to distinguish the different axes.

Table 3.1: Octahedral deformations for the different phases of $NaTaO_3$

	Octahedral lengths (Å)			Inner angles		
Phase	L_x	L_y	L_z	ϕ_x	ϕ_y	ϕ_z
$P4/mbm$	1.977	1.977	1.978	90.0	90.0	90.0
$I4/mmm$	1.978	1.978	1.978	89.7	90.0	89.7
$Im\bar{3}$	1.978	1.978	1.978	90.0	90.0	90.0
$I4/mcm$	1.978	1.978	1.978	89.9	90.0	89.9
$Imma$	1.979	1.979	1.976	89.2	89.7	89.7
$R\bar{3}c$	1.978	1.978	1.978	89.4	89.4	89.4
$Pnma$	1.980	1.980	1.980	89.7	89.5	89.6

Table 3.2: Octahedral deformations for the different phases of $LaAlO_3$

	Octahedral lengths (Å)			Inner angles		
Phase	L_x	L_y	L_z	ϕ_x	ϕ_y	ϕ_z
$P4/mbm$	1.892	1.892	1.892	90.0	90.0	90.0
$I4/mmm$	1.892	1.892	1.892	90.0	90.0	90.0
$Im\bar{3}$	1.892	1.892	1.892	90.0	90.0	90.0
$I4/mcm$	1.902	1.902	1.902	89.9	90.0	89.9
$Imma$	1.903	1.904	1.904	89.3	89.9	89.9
$R\bar{3}c$	1.904	1.904	1.904	89.5	89.5	89.5
$Pnma$	1.904	1.903	1.904	89.9	89.3	89.9

Table 3.3: Octahedral deformations for the different phases of $SrTiO_3$

	Octahedral lengths (Å)			Inner angles		
Phase	L_x	L_y	L_z	ϕ_x	ϕ_y	ϕ_z
$P4/mbm$	1.945	1.945	1.946	90.0	90.0	90.0
$I4/mmm$	1.945	1.945	1.945	89.9	89.9	89.9
$Im\bar{3}$	1.945	1.945	1.945	90.0	90.0	90.0
$I4/mcm$	1.947	1.947	1.947	89.9	90.0	89.9
$Imma$	1.947	1.947	1.945	89.1	89.8	89.8
$R\bar{3}c$	1.947	1.947	1.947	89.8	89.8	89.8
$Pnma$	1.947	1.946	1.947	89.9	89.7	89.9

The results in the tables 3.1, 3.2 and 3.3 show that the octahedral lengths are very similar for all three directions. The biggest difference between octahedral lengths is of the order of 0.01 Å. The inner angles are also very close to 90° with the biggest difference being 0.6°. This means that the octahedral deformations are indeed negligible compared to the tiltings. This can be interpreted as the octahedral bonds being very strong and requiring a lot of energy to be deformed.

From this tables (see Tables 3.1, 3.2 and 3.3) one can conclude that, for $NaTaO_3$, $LaAlO_3$ and $SrTiO_3$, octahedral deformations are negligible compared to the tiltings.

Tilting coordinates:

The following tables show the distortion coordinates for the different phases of the compounds $NaTaO_3$, $LaAlO_3$ and $SrTiO_3$. The coordinates are given in units of Å. The coordinates are defined as the projection of the displacement of the X anions from the position they would have in the cubic phase (see Figure 3.8). Note that in these tables the $Pnma$ phase is denoted as $Pnma'$ to clarify that this is the $Pnma$ phase with the A-ions fixed in place. The same notation is used to differentiate $Imma$ (with freedom of movement in A) from $Imma'$ (with the A-ion fixed).

Table 3.4: distortion coordinates of the different phases of the compound $NaTaO_3$. The $'$ symbol next to some of the space groups indicates that this coordinates have been obtained for the system with the A-ion fixed in the same place as for the cubic phase.

Phase	Q_x (Å)	Q_y (Å)	Q_z (Å)
$P4/mbm$	0.395	0.000	0.000
$I4/mmm$	0.294	0.294	0.000
$Im\bar{3}$	0.322	0.322	0.322
$I4/mcm$	0.399	0.000	0.000
$Imma'$	0.289	0.289	0.000
$R\bar{3}c$	0.124	0.124	0.124
$Pnma'$	0.267	0.240	0.240

Table 3.5: distortion coordinates of the different phases of the compound $LaAlO_3$. The $'$ symbol next to some of the space groups indicates that this coordinates have been obtained for the system with the A-ion fixed in the same place as for the cubic phase.

Phase	Q_x (Å)	Q_y (Å)	Q_z (Å)
$P4/mbm$	0.000	0.000	0.000
$I4/mmm$	0.000	0.000	0.000
$Im\bar{3}$	0.000	0.000	0.000
$I4/mcm$	0.210	0.000	0.000
$Imma'$	0.261	0.261	0.000
$R\bar{3}c$	0.129	0.129	0.129
$Pnma'$	0.000	0.158	0.158

Table 3.6: distortion coordinates of the different phases of the compound $SrTiO_3$. The $'$ symbol next to some of the space groups indicates that this coordinates have been obtained for the system with the A-ion fixed in the same place as for the cubic phase.

Phase	Q_x (Å)	Q_y (Å)	Q_z (Å)
$P4/mbm$	0.065	0.000	0.000
$I4/mmm$	0.054	0.054	0.000
$Im\bar{3}$	0.043	0.043	0.043
$I4/mcm$	0.118	0.000	0.000
$Imma'$	0.040	0.040	0.000
$R\bar{3}c$	0.080	0.080	0.080
$Pnma'$	0.001	0.090	0.090

A more in depth analysis of the results will be done in the next section. However, it is interesting to mention that there is no "+" distortion for the compound $LaAlO_3$. This is consistent with the fact that $LaAlO_3$ has a negative frequency in the phonon dispersion diagram for the point R of the reciprocal lattice [31].

The Tables 3.4, 3.5 and 3.6 show that the magnitude of the tiltings is much smaller for $SrTiO_3$ than for $NaTaO_3$ and $LaAlO_3$. This is consistent with the fact that, despite the low temperature stable phase of $SrTiO_3$ is the $I4/mcm$, the phase transition to the cubic phase $Pm\bar{3}m$ occurs at the low temperature of 105 K [32]. This means that the tiltings in $SrTiO_3$ are small and near the cubic phase.

For the compound $SrTiO_3$, the $Pnma$ phase shows a very small displacement in the X direction (see Table 3.6), this indicates that $Pnma$ is very close to the $Imma$ phase.

Finally, it is worth noting that the values of the displacement coordinates are consistent with the tilt-systems in Figure 3.2. This means that a tilt system such as $a^+a^+a^0$ shows an equal displacement in two coordinates and zero displacement in the third (i.e. $Q_x = Q_y$ and $Q_z = 0$).

Movement of the A-ion:

The last thing studied in this subsection is the movement of the A-ion. When the system shifts from the cubic phase to the distorted phases, due to the loss in symmetry, the A-ion is free to move in one or more directions. This movement allows the system to reach lower energy configurations. The movement of the A-ion is determined by the symmetry of the system and therefore can only happen in certain-phases. The phases where the A-ion is free to move are shown in Figure 3.2

The qualitative analysis of the movement of the A-ion has been done following the same procedure as for the tiltings. However, it has been found that the A-ion movement is more complex than expected as in-phase and out-of-phase movements are present (see Fig. 3.10) and therefore three more coordinates would be needed to fully describe the system being the total number of coordinates 12. These coordinates would correspond to the in-phase and out-of-phase tiltings (6 coordinates) and the in-phase and out-of-phase movements of the A-ion (6 coordinates). Due to the exponential growth of the complexity of the system, this work has not been able to study the A-ion movement in depth and has been limited to the study of the tiltings. However, a qualitative study of its importance has been done in the following subsection where the effects of the movement of A have been studied in the results.

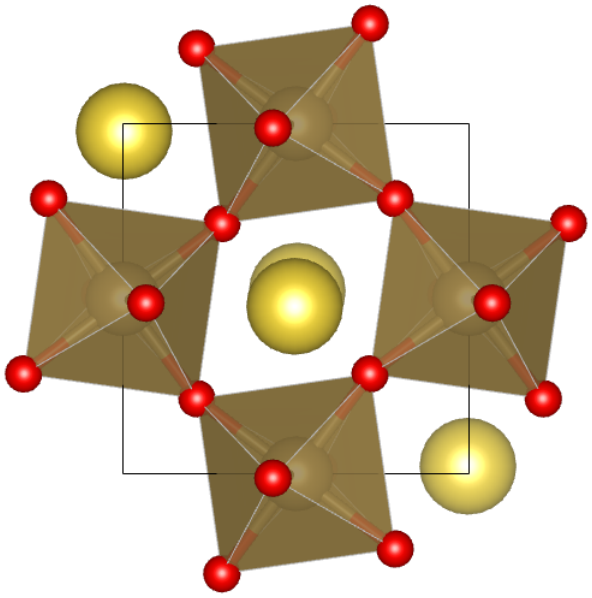

Figure 3.10: This figure shows the *Pnma* phase for the compound $NaTaO_3$. Here, the A-ion (spheres in yellow) show a displacement from their original positions. This displacement is a compound displacement has an X and Y component and is an out-of-phase displacement as two neighbor ions show the same displacement but in opposite directions.

The **conclusions about the geometry of the systems** are the following:

- The **octahedral deformations are negligible** compared to the tiltings. This can be interpreted as the octahedral bonds being very strong and requiring a lot of energy to be deformed comparing to the energy required by rotations.
- The **distortion coordinates are consistent** with the tilt-systems in Figure 3.2.
- The compound **$LaAlO_3$ does not present a "+" distortion** which is consistent with Ref. [31].
- The compound **$SrTiO_3$ presents small tiltings** which is consistent with Ref. [32].
- **For $SrTiO_3$, the *Pnma* phase seems to be very close to the *Imma* phase** as the displacement in the X direction is very small.
- The **movement of the A-ion has been shown to be complex** and therefore is only studied qualitatively in this work.

3.3.3 Numerical results of the simulations: energy and coefficients

In this section the results for the energy of the different phases are shown. The energies are given in units of 10^{-4} eV per unit cell. The energies are given relative to the minimum energy of the system. This means that the minimum energy is set to zero and all other energies are given relative to this value. The tables show the energy for the different phases studied for the compounds $NaTaO_3$, $LaAlO_3$ and $SrTiO_3$.

Table 3.7: Total energies per unit cell for different structural phases of $NaTaO_3$. The *Pnma* phase is found to be the most stable

Phase	Tilt system	Energy per unit cell/10^4 (eV)	$(E - E_{\min})$ (meV)
$Pnma$	$(a^+b^-b^-)$	-1.21063890	0.0
$Pnma'$	$(a^+b^-b^-)$	-1.21063790	104.0
$Imma$	$(a^0b^-b^-)$	-1.21063785	106.0
$Im\bar{3}$	$(a^+a^+a^+)$	-1.21063765	128.0
$R\bar{3}m$	$(a^-a^-a^-)$	-1.21063760	134.0
$Imma'$	$(a^0b^-b^-)$	-1.21063740	151.5
$I4mmm$	$(a^0b^+b^+)$	-1.21063735	156.5
$I4/mcm$	$(a^0a^0c^-)$	-1.21063640	254.0
$P4/mbm$	$(a^0a^0c^+)$	-1.21063610	281.5
$Pm\bar{3}m$	$(a^0a^0a^0)$	-1.21063010	882.5

Table 3.8: Total energies per unit cell for different structural phases of $LaAlO_3$. The $R\bar{3}c$ phase is found to be the most stable.

Phase	Tilt system	Energy per unit cell/10^4 (eV)	$(E - E_{\min})$ (meV)
$R\bar{3}c$	$(a^-a^-a^-)$	-1.35828320	0.0
$Imma$	$(a^0b^-b^-)$	-1.35828300	18.5
$Imma'$	$(a^0b^-b^-)$	-1.35828300	18.5
$Pnma$	$(a^+b^-b^-)$	-1.35828300	18.5
$Pnma'$	$(a^+b^-b^-)$	-1.35828300	18.5
$I4mcm$	$(a^0a^0c^+)$	-1.35828280	39.0
$P4mbm$	$(a^0a^0c^+)$	-1.35828135	185.5
$Pm\bar{3}m$	$(a^0a^0a^0)$	-1.35828135	185.5
$I4mmm$	$(a^0b^+b^+)$	-1.35828135	186.0
$Im\bar{3}$	$(a^-a^-a^-)$	-1.35828135	186.0

Table 3.9: Total energies per unit cell for different structural phases of $SrTiO_3$. The $R\bar{3}c$ phase is found to be the most stable.

Phase	Tilt system	Energy per unit cell/10^4 (eV)	$(E - E_{\min})$ (meV)
$R\bar{3}c$	$(a^-a^-a^-)$	-3.00617430	0.0
$Imma$	$(a^0b^-b^-)$	-3.00617415	10.5
$Pnma'$	$(a^+b^-b^-)$	-3.00617415	11.0
$Imma'$	$(a^0b^-b^-)$	-3.00617415	11.0
$Pnma$	$(a^+b^-b^-)$	-3.00617415	11.5
$I4mcm$	$(a^0a^0c^-)$	-3.00617415	12.0
$P4mbm$	$(a^0a^0c^+)$	-3.00617400	29.5
$Pm\bar{3}m$	$(a^0a^0a^0)$	-3.00617395	35.0
$Im\bar{3}$	$(a^+a^+a^+)$	-3.00617390	37.5
$I4mmm$	$(a^0b^+b^+)$	-3.00617390	38.0

These tables show the minimum energy of the different phases. Unlike for the tables of the distortion coordinates, these tables show the energy both for the phases with and without the A-ion movement despite the fact that only the latter are used to obtain the coefficients of the energy surface. The reason for this is that the phases with A-ion movement are used to validate the model and to obtain a more complete picture of the system. It also shows that the phases where the A-ion is free to move are more stable than the phases where the A-ion is fixed in place. This is expected as the A-ion movement allows the system to reach lower energy configurations.

For $NaTaO_3$ and $LaTaO_3$ the lowest energy phase in the tables (see Tab. 3.7 and Tab. 3.8) corresponds to experimental lowest energy phases being these $Pnma$ and $R\bar{3}c$ respectively [27,29]. However, for $SrTiO_3$ the lowest energy phase in the tables (see Tab. 3.9) is $R\bar{3}c$ which is not the experimentally observed $I4/mcm$ [32]. This is due to the fact that the simulations made give the minimum energy of the band and not the zero point energy which depends on quantum effects. The zero point energy is given by

$$E_0 = E_{min} + \frac{1}{2}\hbar\sum_i \omega_i \tag{3.42}$$

where ω_i are the different frequencies of the phonon modes of the system and E_{min} is the minimum energy of the system. In some cases (see Fig. 3.11), a system can have a lower minimum energy but a higher zero point energy. In the case of $SrTiO_3$, the $I4/mcm$ phase has a zero point energy of $E_0^{I4/mcm} = 0.507$ eV and the $R\bar{3}c$ phase has a zero point energy of $E_0^{R\bar{3}c} = 0.523$ eV.

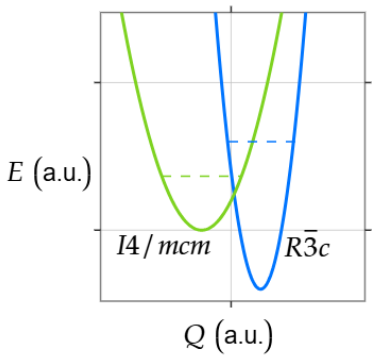

Figure 3.11: This figure shows how it can be possible for a system to have a lower minimum energy but a higher zero point energy. In this figure, the parabolas represent the energy band of each system and the dashed lines the zero point energy. This figure is only qualitative.

Once the energies and coordinates are known, equations (3.39) and (3.41) can be solved to obtain the coefficients of the energy surface. The results of this process are shown in Table 3.10. Note however that if a whole row in the matrix A in equation (3.39) is zero, the corresponding coefficients are not defined as the matrix is singular. This is the case for the coefficients of the in-phase tiltings for $LaAlO_3$. The reason for this is that these compounds do not present in-phase tiltings in any of the phases studied. If the in-phase coefficients cannot be calculated, then the mixed tiltings coefficient H_{+-} cannot be calculated either as it depends on the in-phase coefficients (see equation (3.41)).

Table 3.10: Values for the energy coefficients for the different materials. The K coefficients have units of eV·Å^{-2} and the I and H coefficients of eV·Å^{-4}. However, this units are dropped in this work for notation simplicity.

	In-phase tiltings "+"			Out-of-phase tiltings "-"			Mixed tiltings "+-"
Compound	K_+	I_{++}	H_{++}	K_-	I_{--}	H_{--}	H_{+-}
$NaTaO_3$	-0.695	1.975	2.355	-2.045	10.365	17.110	8.715
$LaAlO_3$	-	-	-	-0.490	3.615	3.620	-
$SrTiO_3$	-0.485	83.565	203.765	-0.670	36.110	39.945	65297.350

A further discussion of the obtained coefficients and their physical meaning (as discussed in Subsection 3.2.2) will be done in Section 3.4. However, a brief analysis of the coefficients can be done here.

As expected, all the force constants K_+ and K_- are negative. This means that the original cubic phase is unstable. However, there is no coefficients for the in-phase tiltings for $LaAlO_3$ as this compound does not present in-phase tiltings (i.e. in that case the cubic phase is more stable than any in-phase tiltings).

As mentioned in Subsection 3.3.2, the tiltings for the compound $SrTiO_3$ are small. This means that the coefficients obtained for this compound are not as reliable as for the other ones as they are obtained from the solutions to an almost singular linear system (see equation (3.39)). This is reflected in the values of the coefficients which are much larger than for the other compounds. Because of this, it has been seen that small changes in the distortion coordinates lead to large changes in the coefficients making these coefficients not very reliable.

The **conclusions about the numerical values for the energy and the coefficients** are the following:

- The movement of the **A-ion lowers the energy of the system**.
- Since the in-phase tiltings for $LaAlO_3$ are not present, **a positive value for the coefficient K_+ can be assumed for $LaAlO_3$** despite the fact that it cannot be calculated by the method used.
- Other than the in-phase distortions in $LaAlO_3$, all the force coefficients are negative meaning that **the cubic phase is unstable**.
- Systems with **small tiltings lead to unreliable coefficients** as the linear systems used to obtain the coefficients are almost singular (see equation 3.39). This is the case for **$SrTiO_3$**.

3.4 Validation of the model and interpretation of the results

This section is dedicated to the validation of the theoretical model proposed in Sections 3.1 and to the study of whether the conditions proposed in Subsection 3.2.2 hold for the numerical results obtained in Subsection 3.3.3.

In order to analyze systems with purely in-phase or out-of-phase tiltings, H and I coefficients must be taken into account. More precisely, the conditions $H > 2I$ or $H < 2I$ must be studied. To do this, the values $H_{++}/2I_{++}$ and $H_{--}/2I_{--}$ are calculated for the in-phase and out-of-phase tiltings respectively. This way, the pure phase stability of a compound is given by a single point $(H_{++}/2I_{++}, H_{--}/2I_{--})$. These points are shown in Figure 3.12 for the three compounds studied in this work.

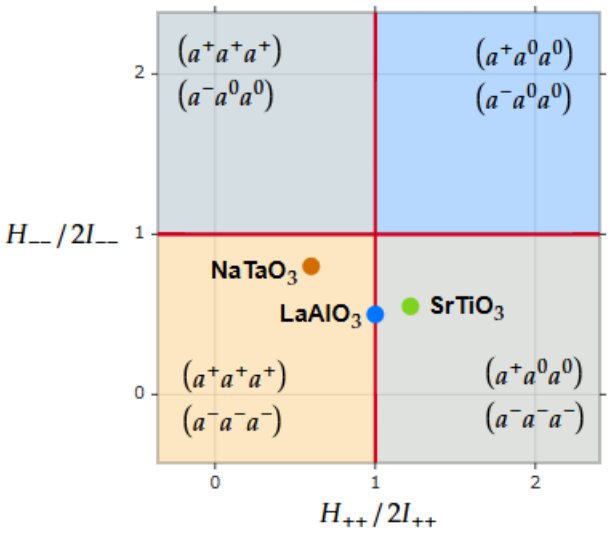

Figure 3.12: This figure shows the different regions for pure in-phase and out-of-phase stability. The three perovskites studied are plotted as points of equation $(H_{++}/2I_{++}, H_{--}/2I_{--})$. For $NaTaO_3$ this point is $(0.59, 0.83)$, for $LaAlO_3$ the point is $(1, 0.50)$ and for SrTiO3 $(1.22, 0.55)$. The value of $H_{++}/2I_{++}$ for $LaAlO_3$ has been set to 1 in order to illustrate that it is not stable for the in-phase tiltings.

The pure tilting approximation is consistent with the numerical results for $LaAlO_3$ and $SrTiO_3$. For $LaAlO_3$, given the coefficients in Table 3.10, according to the relation in Subsection 3.2.2, the most stable phase is $R\bar{3}c$ which is consistent with the numerical results in Table 3.8. For $SrTiO_3$, according to the relation in Subsection 3.2.2, the most stable phases are $P4/mbm$ for in-phase tiltings and $Im\bar{3}$ for out-of-phase tiltings and in fact, these phases are the most stable ones in Table 3.9 for their corresponding pure tilting systems.

For $NaTaO_3$ the model and the numerical results match for the in-phase tiltings as $Im\bar{3}$ is the most stable phase for the pure in-phase tiltings. However, for the out-of-phase tiltings, according to the pure tilting approximation, the most stable phase is $R\bar{3}m$. However, the numerical results show that the most stable phase among the out-of-phase tiltings is $Imma$. This result is however consistent with the addition of the A-ion movement (see Figure 3.7). In this case, $2I_{--} = 20.73$ and $H_{--} = 17.110$ are sufficiently close in value to allow the A-ion movement to stabilize the $Imma$ phase.

Following the reasoning in Subsection 3.2.2, the stability of $Pnma$ can now be analyzed. However, this analysis will only be done for $NATaO_3$. On one hand, since no pure in-phase tiltings are present in $LaAlO_3$, the stability of $Pnma$ cannot be analyzed as it was analyzed in Subsection 3.2.2 since the process requires the in-phase coefficients to be defined. On the other hand, $SrTiO_3$ presents a large change in the distortion coordinates between $P4/mbm$ and $Pnma$ being $Q_a = 0.065$Å in $a^+c^0c^0$ and $Q_a = 0.001$Å in $a^+b^-b^-$ (see Table 3.6). Therefore, the hypothesis that Q_a and Q_b must be similar from the parent phase to the $Pnma$ (see Subsection 3.2.2) phase does not hold for $SrTiO_3$. On top of that, the coefficient H_{+-} is very large for $SrTiO_3$ (see Table 3.10) which means that the mixed tiltings are not expected to be stable. In fact, when looking at the energies in Table 3.9, and the distortion coordinates in Table 3.6, it can be seen that the $Pnma$ phase stabilizes in a $Imma$ configuration with a very small Q_a ($Q_a = 0.001$Å).

In order to analyze $NaTaO_3$, the values of the relevant coefficients and distortions are given in Table 3.11. The values for the quadratic coefficients are calculated using equation 3.36 and the values for Q_a and Q_b are taken from Table 3.4. If the quadratic coefficient is negative, then the transition is energetically beneficial to the system and the change in energy is calculated using equation 3.37.

Table 3.11: This table shows the values for quadratic coefficient from equation 3.36 (i.e. $(2H_{+-}Q_a^2 - 2K_-)$ and $(2H_{+-}Q_b^2 - K_+)$). If this value is negative then that transition is energetically beneficial to the system and the change in energy is calculated (see equation 3.37). The values for Q_a and Q_b are the ones for $Pnma$ in Table 3.4, $Q_a = 0.267$Åand $Q_b = 0.240$Å

Transition	Quadratic coefficient	Change in energy (meV)
$(a^+c^0c^0) \rightarrow (a^+b^-b^-)$	-2.847	195.6
$(c^0b^-b^-) \rightarrow (a^+b^-b^-)$	0.709	-

With these results, when subtracting the change in energy from the energy of the $(a^+c^0c^0)$ phase, the obtained energy is still 85.9 meV higher than the energy of the $Pnma$ phase (see Table 3.7). However, the change in energy is large enough to be lower than the next lowest energy phase, $Imma$ (see Table 3.7). This means that the motion of the A-ion (not taken into account in the development in Subsection 3.2.2) is also responsible for the lower energy of the $Pnma$ phase.

To conclude this Subsection, the results discussed are summarized:

- The **pure tilting approximation is consistent with the numerical results for $LaAlO_3$ and $SrTiO_3$**.
- The motion of the **A-ion is responsible for the stabilization of the** $Imma$ phase in $NaTaO_3$.
- A **large value of** H_{+-} **means that the mixed tiltings are not stable**. This is the case for $SrTiO_3$.
- **The study of mixed tiltings using equation** (3.36) **is consistent with the numerical results** for $NaTaO_3$.
- The **A-ion movement is in part responsible for the stabilization of the** $Pnma$ **phase** in $NaTaO_3$.

Chapter 4

Conclusions

In this work, a model based on Ginzburg-Landau theory has been developed using group theory and symmetry arguments to describe the electronic energy surface of perovskites undergoing octahedral rotations. This model has been complemented with first-principle simulations to obtain the quantitative values for the different parameters of the model for three distinct perovskites: $NaTaO_3$, $LaAlO_3$ and $SrTiO_3$. The model and the simulations have been used complementarily to gain an understanding on the terms that govern the stability of different structural phases.

One of the main results of this work has been precisely understanding the relevant coefficients for the stability of the different phases for the case of pure tiltings (only in-phase or out-of-phase) and understanding the importance of the displacement of the A-ion in the stability of the phases. In fact, the movement of the A-ion plays a key role in stabilizing the *Pnma* phase. This points in a new direction for the study of why this phase is the most stable phase for many perovskites.

Moreover, the results demonstrate that a systematic approach based on Ginzburg-Landau theory and using symmetry can be useful to study the stability of the different phases of the perovskites. In fact, the model has been shown to be valid for the perovskites $LaAlO_3$, $SrTiO_3$ and $NaTaO_3$.

The main results of this work can be summarized in the following points:

- The analytical model neglecting the A-ion movement has been shown to be valid for $LaAlO_3$ and $SrTiO_3$ where the A-ion movements are negligible compared to the tiltings.
- A general understanding of the stability of the different phases has been obtained by analyzing the coefficients of the energy surface.
- The A-ion movement has been shown to be relevant in the stability of the *Pnma* phase.
- The A-ion movement has been shown to be complex and intricate and some guidelines have been proposed on how it should be studied.

To summarize, this work shows that a symmetry-based Ginzburg-Landau approach, complemented by *ab initio* is a powerful tool to investigate the phase behavior of perovskites. The results obtained in this work can be used as a starting point for further studies on the stability of the different phases of perovskites or similar materials. In particular for perovskites, the importance of the A-ion movement has been shown to be relevant in the stability of the *Pnma* phase and therefore it should be studied in more detail in future works.

The following future works are suggested:

- A more detailed study of the A-ion movement, taking into account the in-phase and out-of-phase movements of the A-ion.
- A physical interpretation of the coefficients of the energy surface; how do they relate to the chemical structure and the physical conditions such as temperature and pressure.
- A study of the stability of the *Pnma* phase. Now that the important terms for the stabilization of this phase have been identified, is there a way to relate this terms with the chemical structure of the perovskite? Is there a way to predict which perovskites will have a stable *Pnma* phase?
- Further validation of the model with more perovskites and different phases. The model has been shown to be valid for the perovskites studied in this work, but it would be interesting to see if it holds for other perovskites.
- A similar approach to the one used in this work could be used to study other materials with different distortions.

Bibliography

[1] R. E. Cohen. Origin of ferroelectricity in perovskite oxides. *Nature*, 358:136–138, 1992.

[2] Sk Shamim Hasan Abir, Shyam Sharma, Prince Sharma, Surya Karla, Ganesh Balasubramanian, Johnson Samuel, and Nikhil Koratkar. Piezoelectricity in chalcogenide perovskites. *Nature Communications*, 15:5768, 2024.

[3] N. Hoffmann, T. F. T. Cerqueira, J. Schmidt, A. Rauchenzauner, M. Amsler, S. Goedecker, S. Csányi, C. Wolverton, M. A. L. Marques, L. M. Schoop, M. Scheffler, and C. Carbogno. Superconductivity in antiperovskites. *npj Computational Materials*, 8:150, 2022.

[4] Asish K. Kundu. *Magnetic Perovskites: Synthesis, Structure and Physical Properties.* Engineering Materials. Springer, 2016.

[5] Xiaolin Zhu, Yixiong Lin, Jovan San Martin, Yue Sun, Dian Zhu, and Yong Yan. Lead halide perovskites for photocatalytic organic synthesis. *Nature Communications*, 10(1):2843, 2019.

[6] Carlito S. Ponseca, Tom J. Savenije, Mohamed Abdellah, Kaibo Zheng, Arkady Yartsev, Tobjörn Pascher, Tobias Harlang, Pavel Chabera, Tonu Pullerits, Andrey Stepanov, Jean-Pierre Wolf, and Villy Sundström. Organometal halide perovskite solar cell materials rationalized: Ultrafast charge generation, high and microsecond-long balanced mobilities, and slow recombination. *Journal of the American Chemical Society*, 136(14):5189–5192, April 2014.

[7] Ossila Ltd. Perovskite solar cell efficiencies. `https://www.ossila.com/pages/perovskite-solar-cell-efficiencies`, 2024. Accessed: June 2025.

[8] K. Momma and F. Izumi. Vesta 3 for three-dimensional visualization of crystal, volumetric and morphology data. *Journal of Applied Crystallography*, 44:1272–1276, 2011.

[9] G. Burns and et al. A structural phase-transition in $k(mg_{1-x}cu_x)f_3$ perovskite. *Journal of Solid State Chemistry*, 123(2):467–472, 1996.

[10] R. J. Angel, J. Zhao, and N. L. Ross. General rules for predicting phase transitions in perovskites due to octahedral tilting. *Physical Review Letters*, 95:025503, 2005.

[11] H. D. Megaw. *Crystal Structures: A Working Approach.* W. B. Saunders Company, London, 1973.

[12] K. Uchino. Ferroelectric devices. *CRC Press*, page Cap. 1: Barium Titanate and Lead Zirconate Titanate, 2009.

[13] S. A. Prosandeev and L. Bellaiche. Phase transitions in perovskite ferroelectrics from first principles. *Journal of Materials Science*, 41:245–251, 2006.

[14] Satiye Korkmaz and afşin Kariper. Batio3-based nanogenerators: Fundamentals and current status. *Journal of Electroceramics*, 11 2021.

[15] Toraya Fernández-Ruiz, Inés Sánchez-Movellán, Juan María García-Lastra, Miguel Moreno, José Antonio Aramburu, and Pablo García-Fernández. Many-body model for the cooperative jahn-teller effect in crystals and its associated orbital ordering. *Physical Review B*, 109:205150, 2024.

[16] A. J. Millis, B. I. Shraiman, and R. Mueller. Dynamic jahn-teller effect and colossal magnetoresistance in $la_{1-x}sr_xmno_3$. *Physical Review Letters*, 77:175–178, 1996.

[17] Toraya Fernández-Ruiz, Inés Sánchez-Movellán, Juan María García-Lastra, Miguel Moreno, José Antonio Aramburu, and Pablo García-Fernández. Strain–phonon cooperation as a necessary ingredient to understand the jahn–teller effect in solids. *Journal of Physical Chemistry Letters*, 16(7):1201–1209, 2025.

[18] Ya Gao, Jianjun Wang, Liang Wu, Shanyong Bao, Yang Shen, Yuanhua Lin, and Cewen Nan. Tunable magnetic and electrical behaviors in perovskite oxides by oxygen octahedral tilting. *Science China Materials*, 58(4):302–312, 2015.

[19] H. D. Zhou and J. B. Goodenough. Thermal evolution of the structure and octahedral tilting in $laalo_3$. *Physical Review B*, 81:224117, 2010.

[20] B. J. Kennedy, B. A. Hunter, and C. J. Howard. Structural investigations of $catio_3$ at high temperatures using neutron powder diffraction. *Journal of Solid State Chemistry*, 142:319–327, 1999.

[21] H. D. Megaw. Crystal structures of double oxides of the perovskite type. *Proceedings of the Royal Society of London. Series A*, 58:133–152, 1946.

[22] A. M. Glazer. The classification of tilted octahedra in perovskites. *Acta Crystallographica Section B*, 28(11):3384–3392, 1972.

[23] P. M. Woodward. Octahedral tilting in perovskites. i. geometrical considerations. *Acta Crystallographica Section B: Structural Science*, 53(1):32–43, 1997.

[24] C. J. Howard and H. T. Stokes. Group-theoretical analysis of octahedral tiltings in perovskites. *Acta Crystallographica Section B: Structural Science*, 54(6):782–789, 1998.

[25] Victor M. Goldschmidt. Die gesetze der krystallochemie. *Die Naturwissenschaften*, 14(21):477–485, 1926.

[26] P. M. Woodward. Octahedral tilting in perovskites. ii. structure stabilizing forces. *Acta Crystallographica Section B: Structural Science*, 53(1):44–66, February 1997.

[27] M. Ahtee and C. N. W. Darlington. Structures of $NaTaO_3$ by neutron powder diffraction. *Acta Crystallographica Section B*, 36(5):1007–1014, May 1980.

[28] Yu-Liang Liu, Chuan-Lu Yang, Mei-Shan Wang, Xiao-Guang Ma, and You-Gen Yi. Te-doped perovskite natao3 as a promising photocatalytic material for hydrogen production from water splitting driven by visible light. *Materials Research Bulletin*, 107:125–131, 2018.

[29] I.S. Silveira, N.S. Ferreira, and D.N. Souza. Structural, morphological and vibrational properties of laalo3 nanocrystals produced by four different methods. *Ceramics International*, 47(19):27748–27758, 2021.

[30] Muhammad Rizwan, Samina Gul, Tahir Iqbal, Uzma Mushtaq, M Hassan Farooq, Muhammad Farman, Rabia Bibi, and Mohsin Ijaz. A review on perovskite lanthanum aluminate (laalo3), its properties and applications. *Materials Research Express*, 6(11):112001, sep 2019.

[31] R. Vali. Phonons and heat capacity of laalo3. *Computational Materials Science*, 44(2):779–782, 2008.

[32] Christopher J. Howard, Gregory R. Lumpkin, Ronald I. Smith, and Zhaoming Zhang. Crystal structures and phase transition in the system srtio3–la2/3tio3. *Journal of Solid State Chemistry*, 177(8):2726–2732, 2004.

[33] Maryam RaeisianAsl, Shirzad Jouybar, Saeedeh Sarabadani Tafreshi, and Leila Naji. Exploring the key features for enhanced srtio3 functionality: A comprehensive overview. *Materials Today Sustainability*, 29:101072, 2025.

[34] Dipanjan Sen, Harikrishnan Ravichandran, Mayukh Das, Pranavram Venkatram, Sooho Choo, Shivasheesh Varshney, Zhiyu Zhang, Yongwen Sun, Jay Shah, Shiva Subbulakshmi Radhakrishnan, Akash Saha, Sankalpa Hazra, Chen Chen, Joan M. Redwing, K. Andre Mkhoyan, Venkatraman Gopalan, Yang Yang, Bharat Jalan, and Saptarshi Das. Multifunctional 2d fets exploiting incipient ferroelectricity in freestanding $srtio_3$ nanomembranes at sub-ambient temperatures. *Advanced Materials*, 2025. in press.

[35] P.C. Hohenberg and A.P. Krekhov. An introduction to the ginzburg–landau theory of phase transitions and nonequilibrium patterns. *Physics Reports*, 572:1–42, 2015. An introduction to the Ginzburg–Landau theory of phase transitions and nonequilibrium patterns.

[36] F. Jensen. *Introduction to Computational Chemistry*. Wiley, 2017.

[37] A. Szabo and N. S. Ostlund. *Modern quantum chemistry: Introduction to advanced electronic structure theory*. Dover Publications, 1989.

[38] P. Hohenberg and W. Kohn. Inhomogeneous electron gas. *Physical Review*, 136:B864–B871, 1964.

[39] W. Kohn and L. J. Sham. Self-consistent equations including exchange and correlation effects. *Physical Review*, 140:A1133–A1138, 1965.

[40] W. Koch and M. C. Holthausen. *A Chemist's Guide to Density Functional Theory*. Wiley-VCH, 2001.

[41] L. H. Thomas. The calculation of atomic fields. *Mathematical Proceedings of the Cambridge Philosophical Society*, 23(5):542–548, 1927.

[42] E. Fermi. Un metodo statistico per la determinazione di alcune prioprietà dell'atomo. *Accademia Nazionale dei Lincei*, 6(6):602–607, 1927.

[43] F. Bloch. Bemerkung zur elektronentheorie des ferromagnetismus und der elektrischen leitfähigkeit. *Z. Physik*, 57:545–555, 1929.

[44] P. A. M. Dirac. Note on exchange phenomena in the thomas atom. *Mathematical Proceedings of the Cambridge Philosophical Society*, 26(3):376–385, 1930.

[45] Roberto Dovesi, Bartolomeo Civalleri, Roberto Orlando, Claudio Roetti, Vincenzo R. Saunders, Cristiana M. Zicovich-Wilson, Lorenzo Maschio, Matteo Rérat, Benjamin Montanari, and Nick M. Harrison. Crystal17: A program for the ab initio investigation of crystalline solids. *International Journal of Quantum Chemistry*, 114(19):1287–1317, 2018.

[46] P. García-Fernández, S. Ghosh, N.J. English, and J.A. Aramburu. Benchmark study for the application of density functional theory to the prediction of octahedral tilting in perovskites. *Physical Review B*, 86(14):144107, 2012.

[47] Isaac B. Bersuker. *The Jahn-Teller Effect*. Cambridge University Press, 2006.

[48] M. S. Dresselhaus, G. Dresselhaus, and A. Jorio. *Group Theory: Application to the Physics of Condensed Matter*. Springer, 2008.

[49] J. S. Griffith. *The Theory of Transition-Metal Ions*. Cambridge University Press, London & New York, reissue edition, 1961.